SMARTPHONE-BASED MOLECULAR SENSING FOR ADVANCED CHARACTERIZATION OF ASPHALT CONCRETE MATERIALS

A Thesis

presented to

the Faculty of the Graduate School
at the University of Missouri-Columbia

In Partial Fulfillment

of the Requirements for the Degree

Master of Science

---

by

Sayedomidreza Davami

Amir H. Alavi, Ph.D., Thesis Supervisor

December 2018

The undersigned, appointed by the dean of the Graduate School have examined the thesis entitled

Smartphone-based Molecular Sensing for Advanced Characterization of Asphalt Concrete Materials

presented by Sayedomidreza Davami,

a candidate for the degree of Master of Science
And hereby certify that, in their opinion, it is worthy of acceptance.

Dr. Amir H. Alavi

Dr. Bill Buttlar

Dr. Matt Maschmann

Dr. Carlos Sun

ACKNOWLEDGEMENTS

I would like to express my sincere gratitude to my adviser Dr. Amir Alavi, who offered his continuous advice and encouragement throughout the course of this research. I would like to thank Dr. Bill Buttlar for his guidance throughout this project and innovative ideas, and Dr. Matt Maschmann for his interest in my research. I am thankful for the assistance provided by Dr. Sun, and for his help through course works and advising for the beginning semester.

I would like to acknowledge the contributions of my colleague Behnam Jahangiri who helped me throughout this project. Finally, I greatly appreciate the assistance from Jim Meister because of his all-time help in the Mizzou Asphalt Pavement and Innovation Laboratory (MAPIL). I am also thankful to Asif Gil from Consumer Physics Inc. for his technical supports for the implementation of the SCiO sensor.

TABLE OF CONTENTS

LIST OF FIGURES

LIST OF TABLES

SMARTPHONE-BASED MOLECULAR SENSING FOR ADVANCED CHARACTERIZATION OF ASPHALT CONCRETE MATERIALS

ABSTRACT

Pavement systems deteriorate with time due to the aging of materials, excessive use, overloading, climatic conditions, inadequate maintenance, and deficiencies in inspection methods. Proper evaluation of pavement conditions provides important decision-support to implement preventative rehabilitation. This study presents an innovative smartphone-based monitoring method for advanced characterization of asphalt concrete materials. The proposed method is based on deploying a pocket-sized near-infrared (NIR) molecular sensor that is fully integrated with smartphones. The NIR spectrometer illuminates a sample with a broad-spectrum of near-infrared light, which can be absorbed, transmitted, reflected, or scattered by the sample. The light intensity is measured as a function of wavelength before and after interacting with the sample. Thereafter, the diffuse reflectance, a combination of absorbance and scattering, caused by the sample is calculated. This portable smartphone-based NIR method is used to detect asphalt binders with various performance grading (PG) and aging levels. To this end, a number of binder samples are tested in a wavelength range of 740 to 1070 nm. The results indicate that asphalt binders with different grades and aging levels yield significantly different spectrums. These distinctive spectrums can be attributed to the variations of binder components such as saturate, asphaltenic, resin, and aromatic. Furthermore, the molecular sensor is successfully deployed to detect and classify asphalt mixtures fabricated with a various binder and recycled material types such as styrene-butadiene-styrene (SBS), ground tire rubber (SBS), engineered crumbed rubber (ECR), reclaimed asphalt pavement (RAP), and recycled

asphalt shingles (RAS). The proposed monitoring technology is not only a viable tool for asphalt material characterization but also a cost-effective platform capable of transforming the current physical and chemical methods for civil engineering material characterization.

CHAPTER 1.

INTRODUCTION

1-1. Background and State of Knowledge

In the United States, age-related degradation, deferred maintenance, natural disasters, and manmade hazards have been threatening civil infrastructure systems. Among the hazardous sources, degradation is known as the main cause of failures of civil infrastructures. Recently, the American Society of Civil Engineers (American Society of Civil Engineers 2017), evaluated America's aging infrastructure as a D+ grade. Also, an annual expenditure of $206 billion is estimated in order to improve the overall infrastructure condition and to maintain US global competitiveness by 2025 (American Society of Civil Engineers 2017). Aging and degradation of civil infrastructures in the US have led to a considerable loss in the United States. For instance, roughness (i.e. lack of smoothness) of the major roads in the US resulted in an annual cost of $67 billion on drivers. It is reported that a care which is driven on rough roads needs an additional $349/year comparing to a care which is used on smooth roads (Buttlar and Islam 2014). Therefore, the aged and inefficient infrastructures, especially roads, are considered as serious issues which require advance and forward-looking resolutions. Recently, the development of prominent and innovative monitoring technologies has gained a significant attention in order to evaluate the safety and effectiveness of civil infrastructures. In this regard, the advances in big data analysis and sensor technology could help with coming up with ideas to address the concerns (Lee et al. 2005).

1-2. Pavement Monitoring Systems

Pavement condition is a critical aspect for the development of a country. According to the World Bank, the density of paved roads in good condition varies from 40 km/million inhabitants in low-income economies to 470 middle-income and 8,550 in high-income economies. Moreover, the pavement condition may crucially affect the national budget of a country, both with regard to direct costs, such as road infrastructure construction and maintenance and to the indirect cost such as the social cost coming from the incidental phenomena. Therefore, the knowledge of pavement condition is fundamental to provide safety, comfort, economy and environmental quality in order to satisfy road users. Nowadays, the *Smart Road* concept has been growing thanks to the deployment of advanced technologies and intelligent tools which are able to sense and measure the response of the road structure. As a result, smart pavement health monitoring is becoming an inseparable part of the pavement management system (PMS) to optimize the maintenance strategies and minimize the rehabilitation cost. The service life of most of the major roads in the US is between 5 to 7 years before the first rehabilitation measure. Considering the huge cost of road maintenance and repair works, the service life can hardly last longer than 20 years. This is mainly due to the harsh environmental conditions (such as heavy rains, freezing cycles in winters and hot summers) or the heavy traffic and loads passing over the pavements. That being said, taking timely and appropriate rehabilitation and maintenance measures, the service life can be extended, resulting in a drastic decrease in repair and reconstruction worksa (Schnebele, Cervone, and Waters 2014). Therefore, highway agencies are currently paying remarkable attention to smart and cost-effective tools to collect pavement condition data containing various structural and functional

distresses. Pavement distresses such as rutting and cracking are the among the most detrimental damages to the pavement that adversely affect the rideability and safety of the roads. Lack of adequate inspection and pavement monitoring results in even more detrimental effects of material aging, harsh environmental conditions, and heavy traffic loading. The pavement performance monitoring system should be able to identify the type, extent, and potential causes of failures in order to come up with the most appropriate repair and rehabilitation strategies which lead to the extension of service life of the pavement. Therefore, the first step toward this goal is to know various types of pavement distresses such as cracking (alligator, transverse, slippage etc.), surface deformation (rutting, shoving, corrugations etc.), disintegration (potholes, patches), surface defects (bleeding, raveling, delamination etc.), roughness, surface distress, skid resistance, etc.

1.2.1. Pavement Distresses

1.2.1.1. Cracking

Cracking in asphalt pavement consists of multiple kinds of distresses such as fatigue, block, edge, longitudinal, transverse and reflection cracking. Except for alligator cracking, the main reason and driving force of the distress formation are environmental and climate conditions; although, traffic can contribute to the rate of deterioration. The position, dimension, and orientation of the cracks define the specific type of cracking. Three kinds of cracking including low temperature, block, and fatigue cracking are described below in more details.

Low temperature cracking: This is the most frequently observed distress found in asphalt pavements paved in cold climates such as Canada and northern U.S. Low temperature cracks are mostly perpendicular to the pavement′s centerline or laydown direction (see

Figure 1-1.). This type of cracking is not load associated and environmental conditions drive the crack propagation. Usually a type of thermal cracking. When experiencing low temperatures, the restrained pavement tries to contract. The tensile stresses build up to a critical point at which a crack is formed as the temperature drops. Either a single low temperature event or multiple warming and cooling cycles can cause a low temperature cracking to form. The subsequent cold and freezing days, and also the traffic loading lead to further propagation of the cracks. To address this issue, Superpave set low temperature defined parameters such as stiffness and m-value, which is an indicative of stress relaxation ability) and set criteria for asphalt binder to assure asphalt pavement performance. The procedure to address low temperature cracking via the binder testing is later discussed as bending beam rheometer (BBR) test. However, the binder testing might not suffice to mitigate low temperature cracking and asphalt mixtures might be essential to evaluate and test the cracking resistance of asphalt pavements.

Figure 1-1. An example of very severe low temperature cracking on flexible pavements (Pavement Interactive website)

Block cracking: This is a series of large and perpendicular cracks visible on the surface of an asphalt pavement (see Figure 1-2). This type of cracking typically covers a large area and can be seen in areas where there is no traffic. Block cracking is typically caused by shrinkage (contraction) of the asphalt pavement due to cooling and a drop in temperature. Block cracking is an indication that the asphalt has hardened significantly (Wang and Buttlar 2018). Similar to the thermal cracking, this distress is not a load associated distress. The contraction of asphalt in temperature cycles integrated with the inability of asphalt binder to expand and contract is the main cause of the block cracking formation. The lack of flexibility of asphalt to expand and contract may come from the insufficient or inappropriate binder. Generally, adequate liquid and soft binder can make the proper bond between the high-quality aggregates and provide the structural integrity for the pavement. This deterioration mode is considered in many pavement evaluation guides and condition rating systems such as pavement condition index (PCI) and pavement surface evaluation and rating (PASER).

Figure 1-2. An example of block cracking on flexible pavements (Pavement Interactive website)

Fatigue cracking: This mode of distress is formed as a series of connected cracks due to the fatigue failure of the HMA surface or stabilized base (see Figure 1-3). The repeated loading caused by passages of traffic drives the cracks and make them propagate more. The mechanism of crack formation depends on the structure of the pavement system. In thin pavements, the tensile stress is the highest at the bottom of the asphalt layer. Therefore, cracking initiates at the bottom of the HMA layer then propagates to the surface. *Bottom-up* or *classical* fatigue cracking is the name of this type of fatigue cracking. On the other hand, due to high localized tensile stresses resulting from tire-pavement interaction and asphalt binder aging in thick pavements, the cracks most likely start from the top in areas and then propagate downward. This form of crack propagation is called *top-down cracking*. After repeated loading, the longitudinal cracks connect to each other and form multiple sided sharp-angled pieces that resemble the back of an alligator or crocodile. The alligator cracking is an indicator of structural failure and calls for serious maintenance and rehabilitation. The cracks can also allow moisture penetration and may end up as a pothole.

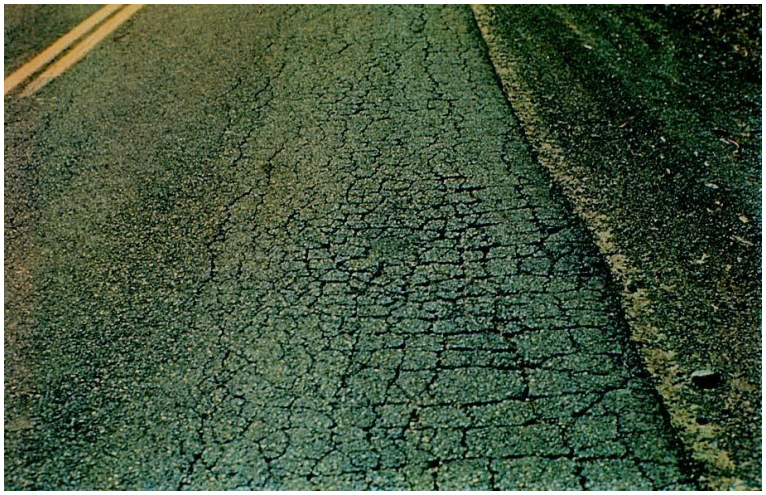

Figure 1-3. An example of very severe fatigue cracking on flexible pavements (Pavement Interactive website)

1.2.1.2. Bleeding

Bleeding is a film of asphalt binder on the pavement surface (see Figure 1-4). It usually creates a shiny, glass-like reflecting surface that can become sticky when dry and slippery when wet. Bleeding asphalt is defined as the upward movement of asphalt in a seal coat or surface treatment that creates a film of asphalt on the surface of roadways. It relates to excess asphalt binder filling empty space in the aggregate mat, this material moves upward to the surface of the asphalt. Then, under the pressure of heat and traffic, it creates a non-reversible problem that worsens over time. When traffic drives over bleeding pavement it creates a smacking sound, similar to the sound made by tires driving over wet pavement. Bleeding is most common during seal coat or surface treatments when the binder has not yet fully cured.

The expansion of the liquid binder due to the hot weather and/or the further compaction of the asphalt pavement due to the passages of traffic may result in the upward movement of the binder. This excessive binder stays on the surface and accumulates. In order to avoid this distress mode, the binder content in the asphalt design should be controlled. It should be taken into account that the lack of sufficient liquid binder should be avoided as it results in cracking problems. In addition, as the liquid binder is the most expensive component in the mixture, excessive binder content impose extra cost on asphalt production. Furthermore, the low air void content does not leave enough room for the expansion of the binder. As the thermal coefficient of expansion and contraction of asphalt binder is higher than aggregates, high enough air void content should be considered in the mix design to mitigate bleeding.

Figure 1-4. An example of bleeding on flexible pavements (Pavement Interactive website)

1.2.1.3. Rutting

Rutting is the surface deformation in the wheel path that cannot be recovered (see Figure 1-5). The viscoplastic nature of this distress makes it irreversible; hence, extra care should be taken to design a pavement system which is resistant to permanent deformation. Ruts are especially visible after a rain and when they are filled with water. Asphalt layer rutting and subgrade layer rutting are the main two types of permanent deformation. Lack of enough compaction and also a soft asphalt mixture may result in ruts on asphalt layer. On the other hand, subgrade rutting may happen due to the heavy loads and also lack of structural integrity. In addition to the road roughness made by rutting, hydro planning endanger the safety of the passengers. As the ruts are filled with surface water, it makes the steering difficult and may lead to car flipping. While the densification of pavement layers can contribute to the rutting, shear failure caused by traffic loading at high temperature is the main reason of rutting. Nowadays, application of recycled materials such

as reclaimed asphalt pavement (RAP), recycled asphalt shingle (RAS), and ground tire rubber (GTR) has made the asphalt pavements stiffer and the rutting distress less crucial. However, adequate compaction effort, deployment of appropriate binder type, and high quality aggregates should be provided in order to mitigate rutting.

Figure 1-5. An example of rutting on flexible pavements (Pavement Interactive website)

1.2.2. Pavement Condition Assessment Indexes

The International Roughness Index (IRI) is a standardized roughness measurement, developed by the World Bank in 1980, which provides a ride quality classification in term of the longitudinal profile, traveled by a wheel path. The IRI is defined as the filtered ratio of the accumulated deviation of the vehicle's suspension divided by the traveled distance. The profile necessary for the calculation of the index can be obtained by any valid measurement instrument, starting from static rod level to high-speed inertial profilers, as reported. Pavement roughness is directly linked to riding quality - comfort and to safety because is one of the causes of load loss accident.

Rut Depth (RD) measures the longitudinal pavement deflection along the wheel path as a consequence of the accumulation of visco plastic deformations of layers and subgrade. The main causes of rutting distress are heavy traffic load repetition or lateral movement of the material of the layers. Rut Depth is an important indicator linked to road safety because during wet weather conditions high rutting level can facilitate the hydroplaning phenomena and loss of control of the vehicles. RD measurement is simple but it needs high accuracy in data acquisition: it can be calculated from profiles obtained with any valid measurement method, ranging from the static rod and level surveying equipment to high-speed inertial profiling systems.

Present Serviceability Index (PSI) is a parameter used to describe the functional condition of pavement with respect to riding quality: it provides a valuation of the ability of the road to serve traffic: it takes into account several road characteristics such as slope variance, rut depth, cracking and patching surfaces. The PSI is used to provide a comprehensive evaluation of pavement conditions, for both safety and comfort aspect: the complexity makes several input data necessary to the calculation.

1.2.3. Current Monitoring Technologies

To determining the optimum pavement maintenance strategies, the distress types should be identified and extend needs to be quantified. Visual inspection of the pavements to assess the readability of the pavements by well-trained pavement experts is the most simple measures that could be taken. Despite the ease of this method, it might result in bios and unreliable data collection and can impose extra cost and time on the project. In addition, it sometimes involves traffic shut-downs and jeopardizing the inspector's safety. As a result,

automated methods of condition assessment of the pavements have been proposed to counterpart the downsides of the visual inspection. To this end, sophisticated equipment and data collection technique are needed to be developed. Thanks to these innovative methods, the production of quantitative analysis of the pavement condition can be possible. Non-subjective, high productivity, and accurate data set are needed to appropriately assess the condition of the pavement and come up with prohibitive measures.

Ground penetrating radar (GPR) has been used as one of the non-destructive methods to monitor the condition of the pavements. Xu and Yang (2018) proposed an innovative application for mobile platforms for real-time GPR data processing. They focused on providing a useful support for engineers and technicians as well, for road and pavement inspection. The application was claimed to play an important role for agencies dealing with roads and highway management. Using the collected data via radar, it provided applicable condition assessment opportunities by improving the on-site efficiency and effectiveness of the works (Xu and Yang 2018)

One of the key parameter in the prediction of the pavement distress is the ability to determine the strain and stress distributions in asphalt pavement. Having the knowledge of the stress and strain level in the pavement structure, the critical points can be detected and the material properties such as stiffness and strength can be chosen to avoid failures in the place of critical weak points. However, there is a need to monitor the already constructed roads to assure the structural efficiency and avoid the failures. To this end, researcher have applied sensors in the pavements detect the response of materials under different traffic loads and environmental conditions. The sensors are normally categorized into two groups, electromagnetic sensors and optical fiber sensors. A study by Rana et al. (2016) showed

that fiber optic sensors (FOS) can be used for civil structural health monitoring. One of the unique features of FOSs is their small size such that they could be embedded within civil structures without any interfere with the efficiency of the structure. In addition, monitoring civil structures at different locations could be achieved due to their distributed sensing technology. The optic nature of the sensor does not allow any electromagnetic interference effect the sensing quality. Finally, not only strain and displacement, but also vibration, cracks, corrosion, and chloride ion concentration could be detected. Despite the aforementioned pros, optical fibers could be fragile and needed to be covered within a protective material. Also, they could not be reused and once they were damaged, there was a low probability for them to get repaired. Figure 1-6 shows the use of Fiber Bragg Grating (FBG) sensor for monitoring of pavements.

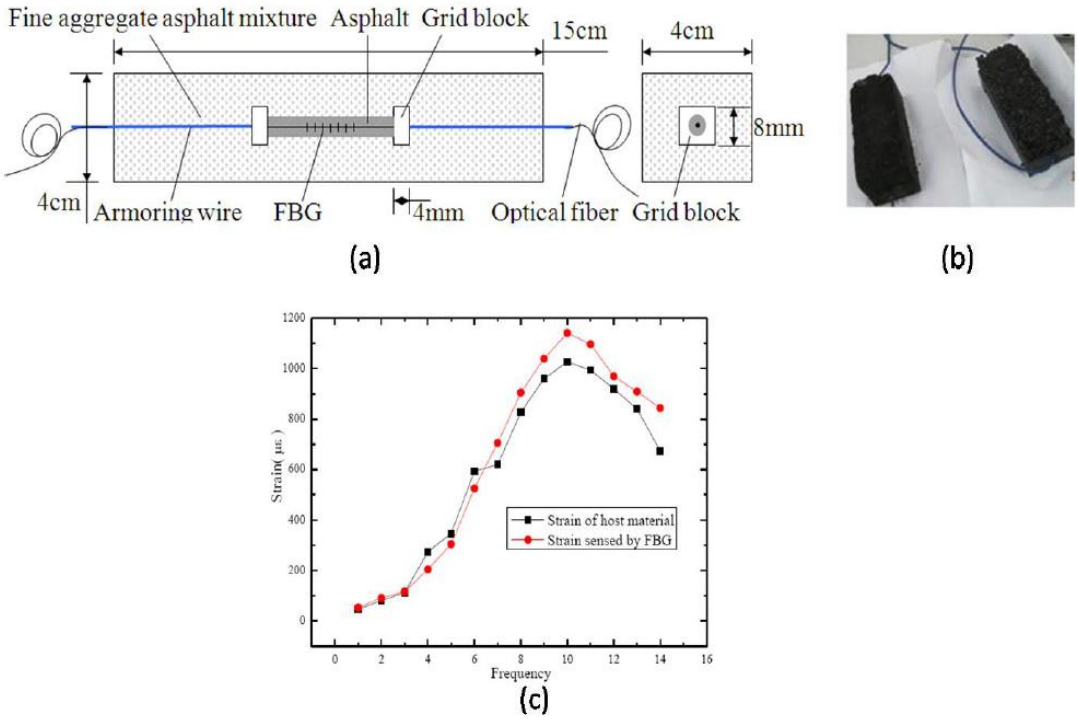

Figure 1-6. Schematic design of fine aggregate asphalt mixture encapsulated (a) fiber optic sensor, (b) real picture, and (c) strain sensing capability (Rana et al. 2016).

A recent study by Augusto et al. (2013) proved the efficiency of Falling Weight Deflectometer (FWD) method. The case study concerned 13 km of a national road rehabilitation in the North of the country. This two-way road, with two lanes in a carriageway, does not have a pavement shoulder. The 13 km of pavement studied were very heterogeneous. Along the pavement, there were some sub-sections of a new structure consisting of a bituminous macadam base course layer and granular layers of extended grading crushed aggregates (ABGE). There were also sections that had been reinforced or widened and consisted of bituminous macadam base and pre-base course layers, with a geotextile at the interface between them, overlaying the old pavement structure. The deflection values registered with the FWD device were normalized to the peak pulse load of 50 kN. Figure 1-7 presents the deflection values obtained for each sensor at every test point.

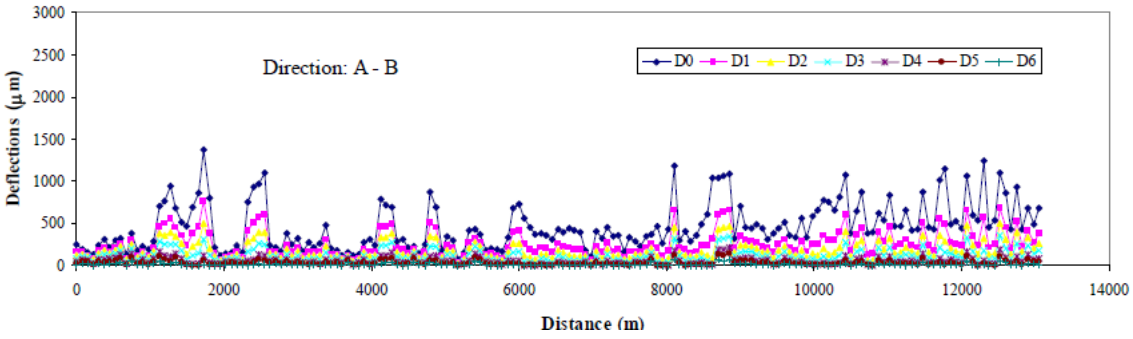

Figure 1-7. Deflections measured in FWD tests perform in the direction A – B (Augusto et al. 2013).

Digital cameras in distress detecting is a mature technique based on using commercially available devices that can acquire 2D images in the visible spectrum of light. The image is

captured through a digital photosensitive sensor CCDs (Charge-Coupled Devices) (Huang 2006; Yu and Salari 2011) or CMOS (Complementary Metal-Oxide Semiconductor) (Yu and Salari 2011). Currently, the two sensors are comparable in performance and usable without any difference, but the CCDs are the most used sensors for the identification of distresses because they are cheaper and have a greater chromatic accuracy. The line-scan camera is ideal for applications requiring both high acquisition rates and high resolution. A line scan camera produces a sequence of single lines pixels, (generally 2000x1 pixel until 8192 pixels per line in higher resolution devices): to build up a two-dimensional image of the pavement, either the camera is moved perpendicular to the line of pixels, generally by a terrestrial vehicle. Line scan camera can assure a high daily productivity in survey phase, in fact, a high frame rate of the camera (such as 28 kHz) allows the vehicle to drive up to 90 km/h, but it can result in a time consuming and expensive post-processing and distress detection phase (Koch, Jog, and Brilakis 2013).

Laser scanner technique is based on LiDAR (Light Detection and Ranging) technology (Chang, Chang, and Liu 2005). It allows obtaining very accurate and high-resolution 3D information of the object scanned by dense point cloud. It is based on two principles: time of flight and phase shift. The time-of-flight sensors estimate the distance between the target and the center of the instrument by the measure of the time elapsed between the emitted and the reflected laser signal, while the phase shift sensors are based on the measurement of the angular offset between the emitted and the reflected signal. Phase shift sensors have a more limited range than those at time of flight (<150m), on the other hand, they have a higher acquisition frequency (more than a million points per second). The accuracy

obtainable with time-of-flight instruments is between 3 and 6 mm @ 100m, values that increase with increasing distance (Bechadergue, Chassagne, and Guan 2016).

For a better understanding of the pavement response, various pavement research facilities (test roads) have become an integral of pavement research and engineering such as the AASHO Road Test conducted in Ottowa, Illinois from 1958 to 1960. As early as in 1989, Rollings and Pittman presented the result of instrumental model tests and full-scale traffic test on the rigid pavement, which matched the Westergaard edge-loaded analytical model well on design stresses. In 2004, eight sections were fully instrumented to measure in situ pavement responses under load at the NCAT test track (David H.Timm, Angela L.Priesr 2004) presented the data collection and processing procedures for the NCAT test track instrumentation. MnROAD in Minnesota was heavily instrumented with 40 test cells; based on the monitored data Lukanen developed mechanistically based load equivalency factors (LEF) in 2005. The Virginia Smart Road is another outdoor pavement research facility located in Blacksburg of Virginia, which has twelve instrumented sections. In another study (Loulizi et al. 2006) used one section of the Virginia Smart Road to compare measured stress and strain, and obtained the difference between the stresses and strains measured in situ and calculated for a flexible pavement section.

1.2.4. Infrared (IR) and Near Infrared (NIR) Spectroscopy

1.2.4.1. Application of Fourier Transform Infrared (FTIR) spectroscopy

Infrared absorbance was applied by Kawahara (1969) to distinguish asphalt binder from crude oil. In this study, some absorbance ratios (e.g. intensity at 810 cm^{-1} absorptions to the intensity of the 1375 cm^{-1}) were reported to be the distinguishing tools between two

petroleum products (Kawahara 1969). In addition to tests such as dynamic shear rheometer (DSR), multiple stress creep recovery (MSCR) rotational viscosity and bending beam rheometer (BBR) which characterize the rheological properties of asphalt binders is Macroscale, Fourier Transform Infrared (FTIR) is widely used to study the characteristics of binder in molecular scale. FTIR is a technique deployed by researchers to obtain the infrared absorbance spectrum, and then characterize the chemical properties of materials in solid, liquid or gas phases. Given the fact that the absorbance of infrared spectra is a function of the molecules' rotational movement at specific frequencies, the functional groups within the material under study can be detected (Yao et al. 2013; Zhu et al. 2018; Jia et al. 2014). FTIR is now believed to be an effective method to detect the grade, source, modifier, and additive detection of asphalt materials (Hou et al. 2018).

Oxidative aging is one of the phenomena that is believed to change the chemical bond between the asphalt binder molecules. This rearrangement in molecular setup may lead to a variation in absorbance or transmittance of the infrared spectrum. The level of the aging is then characterized and quantified using the Infrared spectrum of the aged binder. To this end, the ratio of the intensity of the 1695 cm^{-1} region (attributed to the carbonyl group) to that of 1455 cm^{-1} (attributed to saturated C=C vibrations) was proposed by Negulescu et al. (2006) to determine the relative degree of oxidation of the samples.

Different dosages of automobile waste engine oil were used in asphalt binder containing reclaimed asphalt to investigate the effect of this additive on low temperature performance of asphalt binder (Jia et al. 2014). FTIR testing results showed the presence of similar functional groups and molecular structures in binders containing RAP, and engine oil. However, the absorbance ratio at 1655 over 1455 cm^{-1} was very close to zero. This

observation indicated that the inclusion of oil residues and RAP can lead to more carbonyl functional groups which relate to the oxidation of asphalt binder (Jia et al. 2014).

To show the enhanced aging performance of nano-zinc oxide (nano-ZnO) and organic expanded vermiculite (OEVMT) modified asphalt binders, Zhu et al. (2018) implemented the FTIR spectroscopy. FTIR with a testing range of 4000 to 400 cm^{-1} could detect the differences between 60/80, 80/100 and 100/120 penetration grade asphalt binders after thin film oven test (TFOT) and pressure aging vessel (PAV) aging procedures.

1.2.4.2. Application of Nera Infrared (NIR) spectroscopy in Material Classification

An NIR camera was employed by (Murase and Kato 2018) to investigate the classification capability of near-infrared spectroscopy using images of three different materials, namely, human skin, plant and asphalt binder. Herold (2004) used the NIR with a wavelength of 350 to 2500 nm to characterize the aged asphalt as well as the painted points of asphalt and non-painted parts. Raveling road pavements and regular road pavements were part of his study. Herold (2004) was able to characterize them using the NIR method. Surface treatments happened when asphalt cracks or there were some damages to the area. Surface treatment material was different from the regular binder. Herold (2004) proved the ability of the NIR method to detect the surface treatment area in comparison to the area without surface treatment. It was found that the regular aging of asphalt binder is caused by the reaction of the binder with the atmospheric oxygen and some photochemical reactions with the solar radiation and the influence of freeze-thaw cycles as well as heat results in the aging process.

NIR was used to discriminate different materials by Murase and Kato (2018) using Partial Least Square Regression (PLSR). The wavelength used in this study is 650 to 1050 nm and the materials were plant, skin, and asphalt. A 16-bit Charge-Coupled Device (CCD) camera with a near infra-red tunable filter and a halogen lamp were used in a dark room to take photos of different materials. Chemometric defines as the art of extracting chemical relevant information and characterization from data that was produced in a chemical experiment. Chemometric involves different tools such as Principal Component Analysis (PCA), data pretreatment algorithms, and multivariate calibration methods.

1.3. Research Objectives

In this project, the world's first pocket-sized NIR micro spectrometer will be deployed for advanced characterization of asphalt concrete materials. The NIR spectrometer is fully integrated with the smartphone technology for real-time monitoring. The real-time material characterization analysis service provides testing results instantly via a smartphone app upon scanning of the samples. This is achieved using a cloud-based deep learning algorithm which has been already trained with scanned NIR spectrum data. The beauty of this sensing system is that it can be readily used by citizens for varied material characterization missions. In this method, the NIR spectrometer illuminates a sample with a broad-spectrum of near-infrared light, which can be absorbed, transmitted, reflected, or scattered by the sample. The light intensity is measured as a function of wavelength before and after interacting with the sample. Thereafter, the diffuse reflectance, a combination of absorbance and scattering, caused by the sample is calculated. This portable smartphone-based NIR method is used to detect asphalt binders with various performance grading (PG)

and aging levels. To this end, a number of binder samples are tested in a wavelength range of 740 to 1070 nm. The results indicate that asphalt binders with different grades and aging levels yield significantly different spectrums. These distinctive spectrums can be attributed to the variations of binder components such as saturate, asphaltenic, resin, and aromatic. Furthermore, the molecular sensor is successfully deployed to detect and classify asphalt mixtures fabricated with a various binder and recycled material types such as styrene-butadiene-styrene (SBS), ground tire rubber (SBS), engineered crumbed rubber (ECR), reclaimed asphalt pavement (RAP), and recycled asphalt shingles (RAS).

1.4. Research Scope

This research project deals deployment of a pocket-sized NIR micro spectrometer integrated with the smartphone technology for real-time characterization of asphalt concrete materials.

1.5. Research Approach

The research approach is based on three major stages as follows:

I) Development of a database of the NIR spectra for a range of asphalt binders

II) Development of a database of the NIR spectra for asphalt mixtures with additives such as Reclaimed Asphalt Pavement (RAP), Reclaimed Asphalt Shingles (RAS), and rejuvenators with different properties and percentages.

III) Extracting the patterns of the scanned NIR spectra, and detecting material properties, type of binders without extensive laboratory testing, the percentage of varied additives in hot mix asphalt (HMA), as well as other asphalt distresses such as aging.

CHAPTER 2.

NIR SENSING TECHNOLOGY AND EXPERIMENTAL STUDY

2.1. The NIR Molecular Sensor

In this study, the world's first pocket-sized NIR micro spectrometer, called SCiO, is deployed for characterization of asphalt concrete materials. The SCiO sensor developed by Consumer Physics combines two integrated technological components, the revolutionary sensor that is fully integrated with the smartphone technology, and a powerful cloud computing platform. Together these disruptive technologies provide a comprehensive end to end solution for instant material analysis. The traditional NIR Spectrometer is miniaturized using advances in micro-optical technology. The optical head is only a few millimeters in size and provides sensitivity and accuracy levels on par with the best bench spectrometers. The low power consumption and zero warm-up time make it highly responsive and extremely efficient, allowing it to perform hundreds of scans from a small rechargeable battery. The cloud provides the analytical processing power and hosts the material database. The SCiO cloud hosts the chemometric models and algorithms that analyze spectra and convert them into useful material data. The chemometric models run on a linearly scalable architecture, which allows us to provide fast response times to a practically infinite number of users and devices.

Developer Toolkit offered by Consumer Physics is an easy-to-use tool that enables users to customize SCiO to meet specific material analysis needs. It allows for creating

customized molecular sensing models by collecting spectra of the relevant materials with SCiO and the SCiO Lab Mobile application.

After collecting the required spectra, SCiO Lab Web creates the models, analyzes the spectral data, and generates the algorithm. Models are then deployed in the cloud and used to analyze materials with SCiO devices. Figure 1-2 shows an example of the website interface that provides the access to the scan raw data. It also provides the user with the processing options on the raw data. For example, average, log, and first derivative are among the functions that the user can apply on the raw data for further processing and comparing purposes.

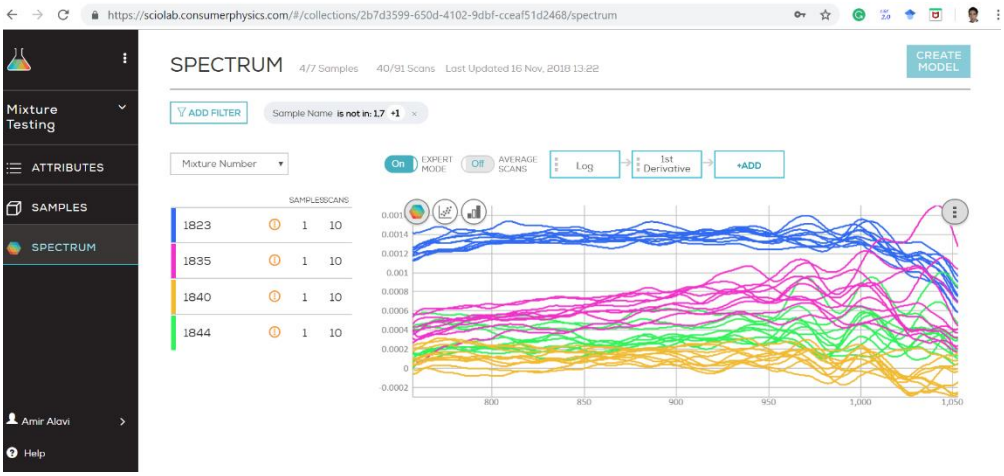

Figure 2-1. Screen shot for the website and workflow used in this research

The SCiO sensor is used to illuminate billions of photons with a wavelength of 740 nm to 1070 nm and another sensor detects the reflectance. The reflectance graph is sent to a mobile device using a Bluetooth sensor and then the phone will send the data to the cloud database in real time using Wi-Fi or Cellular network such as LTE or 3G. The database will analyze the data and compare it to the models that were created before and based on

them it gives the best result (shown in Figure 2-2). Here the important role of good database and model will stand out and makes the difference.

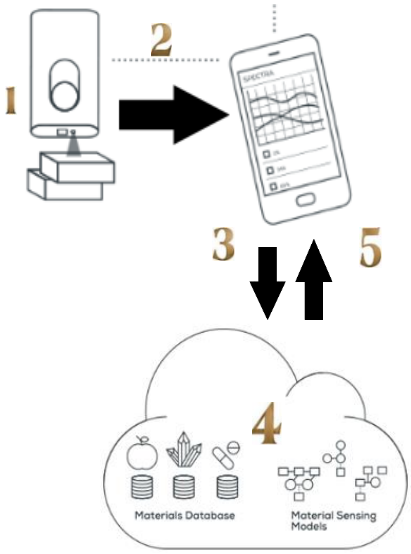

Figure 2-2. Schematic workflow of the research

2.2. Sensor Technology

In this section, the technical details of the SCiO sensor are explained. As shown in Figure 2-3, there are three screws held the Li-Po battery housing to the enclosure, with the PCB sandwiched between. The only real user interfaces are the large, singular button for powering and scanning, the micro USB slot for charging and the charging indicator LED.

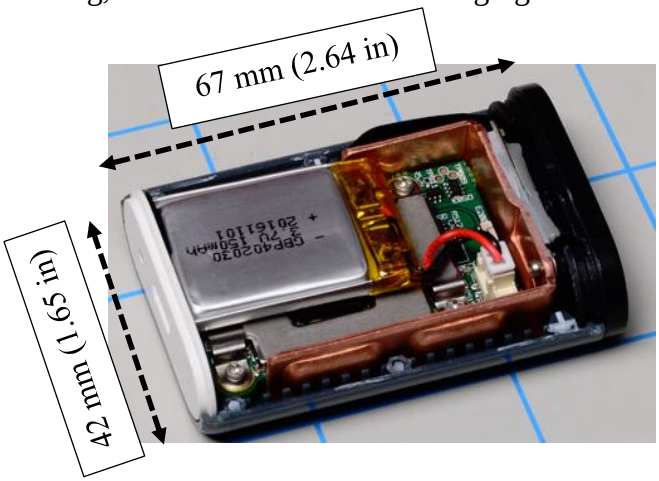

Figure 2-3. Sensor without cover

As shown in Figure 2-4, the most noticeable part of the assembly is a large heatsink wrapped around the PCB and affixed to the imaging sensor with thermally-conductive adhesive. The only item connecting the PCB to the sensor is a flat flex cable assembly with a socket connector on the end.

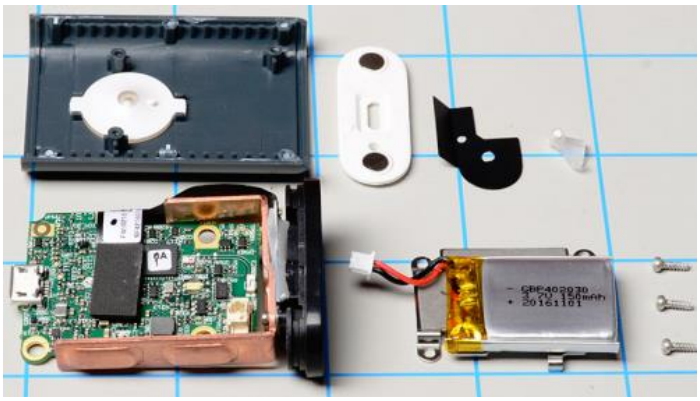

Figure 2-4. Different parts of the sensor

The sensor has an impressive amount of technology packed onto one small board. As shown in Figure 2-5, one side is populated with a majority of the ICs and the user interface button, complete with reverse-mounted LED. The other side is populated with the socket connector for the sensor, micro USB connector, battery connection, Bluetooth® antenna and other various bits and pieces.

Figure 2-5. Main board used in the sensor

An NIR spectrometer the size of an IC is the major technology behind the SCiO. One nice feature of the housing was the magnets embedded within, which allowed for a magnetic bond between the device and its stands, as seen in Figure 2-6.

Figure 2-6. Illuminator and receiver

2.3. Binder Samples and Tests

2.3.1. Aging of the Asphalt Binder

According to the Superpave binder specification, three main stages (aging levels) should be considered to test the liquid binder. The first stage is called original asphalt binder (sometimes called *neat* or *tank binder* as well) and represents the stage at which the binder is transported, stored, and handled prior to mixing with other asphalt mixture ingredients. The second stage represents the aged asphalt binder after asphalt mixture production and construction in a plant (short-term aging). The third stage is represented by an asphalt binder which has undergone a relatively higher level of aging during a long period of service. In this section, the aging process of a liquid binder is described.

2.3.1.1. Rolling Thin Film Oven (RTFO)

The tank binder is short-term aged in the Rolling Thin-Film Oven (RTFO) apparatus (see Figure 2-7) at Mizzou Asphalt Pavement and Innovation Lab (MAPIL) to simulate the aging of binder experienced during the asphalt mixture manufacturing and placement. To this end, the tank binder is exposed to high temperature (163 ℃) and the blow of air through a nozzle is applied as carrousel is rotated at 15 RPM for 85 minutes. The RTFO is an updated version of Thin-Film Oven Test (TFOT) which was previously used for short term aging of asphalt binder. The basics of these two tests are the same except that the TFOT placed tank binder samples in shallow pans which were similar to the pans used for pressure aging vessel (PAV) equipment. The RTFO surpasses TFOT since the fresh binder can be continuously exposed to heat and air flow thanks to the rolling action of the carousel. Also, surface skin is avoided because of the rolling action of the carousel; therefore, the aging is not impeded. The aged binder can then be used for physical property testing and also further levels of aging. In addition, RTFO quantitatively measures the volatiles loss during the aging process by introducing mass loss parameter.

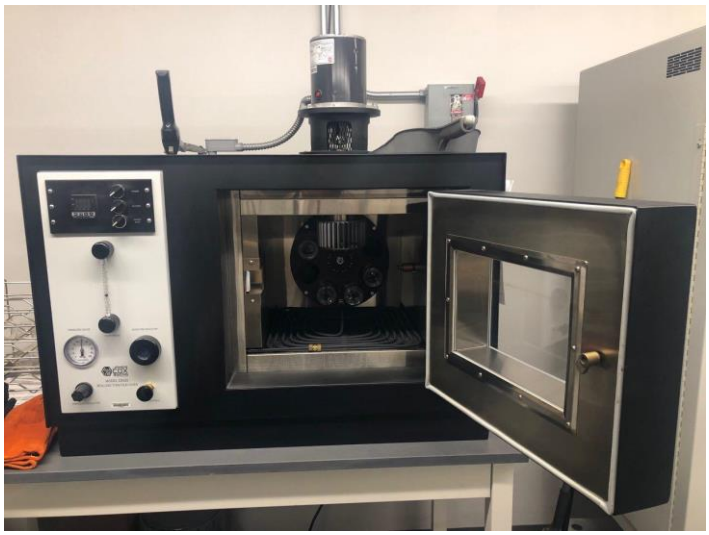

Figure 2-7. Rolling thin-film oven (RTFO) apparatus at MAPIL

In this test, the fresh liquid binder is placed within the cylindrical glass bottles and then the bottles are put in a rotating carriage in the oven. The carriage rotates within the oven while the 325°F (163°C) temperature ages the samples for 85 minutes. This test is performed per AASHTO T 240 and ASTM D 2872. One of the Superpave binder specification goals is to measure the properties and evaluate the performance of a binder in a condition which is as close as possible to the field condition. The hot mix asphalt production and placement are believed to induce the early stage of the aging. During these procedures, the asphalt binder temperature should be high to be properly mixed with aggregates. To evaluate the asphalt binder and asphalt mixture performance in early stages of their lives, a standard aging method of the binder was required. Superpave used the RTFO method to produce aged binders that are supposed to meet some criteria to mitigate fatigue and rutting distresses. Another parameter which is of interest in this test is the loss of volatiles. A change in viscosity of the binder under the aging process in the RTFO test is a result of losing volatiles. This is similar to the process that happens in a real asphalt plant in which the volatiles of the liquid binder are removed because of the elevated temperature.

2.3.1.2. Pressure Aging Vessel (PAV)

Over the life of an in-service asphalt pavement, the asphalt binder, as one of the ingredients of the mixture, slowly ages. In this process, the oxygen from the surrounding environment penetrates through the HMA and chemically reacts. This chemical reaction of the oxygen with the asphalt binder molecules results in aging and hardening of the binder. To simulate long term aging of asphalt binder, the Pressure Aging Vessel (PAV) equipment is used (see

Figure 2-8). The aged binder is then used to test mechanical properties such as stiffness and stress relaxation rate (m-value). In this test, the liquid binder is exposed to elevated temperature and air pressure to simulate in-service aging, around 7 to 10-year period. The PAV test uses the already RTFO aged binders. The short-term aged binder is placed in stainless steel pans and then become long-term aged after 20 hours in a heated vessel pressurized to 2.10 MPa (305 psi). The PAV aged binder is then used to make testing samples to characterize the mechanical properties. This test is performed per AASHTO R 28 standard.

The Superpave PG binder specification required long term aged asphalt binders to be tested at intermediate and low temperatures to determine fatigue and low temperature cracking resistance, respectively. As the asphalt pavement ages, more and more damages initiate or become more severe. To investigate the performance of asphalt in its later stages of service life, a method to simulate aged asphalt binder is important. Various factors contribute to asphalt binder aging. That being said, the key component of concern for the PAV is oxidation. The viscosity of the asphalt binder increases as the oxidation increases. This happens as the age of the binder increases and the chemical components of the binder change. The RTFO aging procedure is used to simulate aging during mixing and placement, while the PAV aging procedure is used to simulate aging during in-service life. Therefore, asphalt binder tests concerned with mix and placement properties (such as the DSR) are conducted on RTFO aged samples, while asphalt binder tests concerned with in-service performance (such as the DSR, BBR) are performed on samples first aged in the RTFO and then in the PAV.

Figure 2-8. Pressure aging vessel (PAV) apparatus at MAPIL

2.3.2. Rotational Viscometer (RV) Test

Viscosity is a temperature dependent property of liquid materials. This parameter is used to describe the resistance of binder to flow. Asphalt binder is viscous at high temperatures and easily tends to flow. As the temperature decrease, binder becomes stiffer and do not flow as easy as it does at high temperatures. The difference in the viscosity of the binder at different temperatures can indicate temperature susceptibility of the binder. High temperature binder viscosity is measured to ensure that the asphalt is fluid enough when pumping. During the pumping process, the binder is not aged. Therefore, the rotational viscosity is measured on unaged or "tank" asphalt. As shown in Figure 2-9, “Brookfield DV3T” rotational viscometer apparatus is used in this study. The apparatus consists of two items: Viscometer and thermoset. Using a motor, the viscometer powers a spindle to rotate

within the chamber containing the binder sample. The speed of rotation can be selected from 0.01 through 250 rpm in steps as small as 0.01 increments. Overall viscosity range capability is 0.1 to 800 million cP (mPa.s) and shear rates from 0.002 to 1875 sec^{-1}. The DV3T is supplied with an accurate RTD probe for monitoring sample temperature. Optional remote probes are available that provide temperature status and enable control of Brookfield accessories.

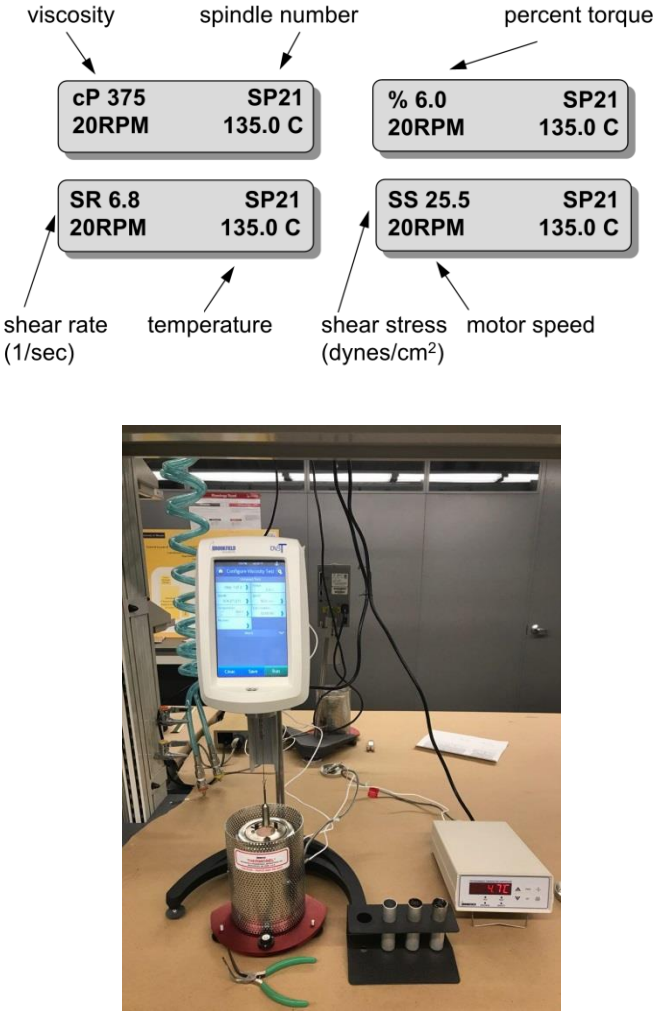

Figure 2-9. RV device and details of its displaying monitor

The RV test is carried out based on ASTM D4402-15. Depending on the spindle size used in this test, a specific amount of binder is poured into the sample chamber. After that, the sample temperature should be raised to the testing temperature within 30 minutes. Then, the binder sample stays at the testing temperature for 10 minutes for temperature equilibrium. Finally, the motor starts and spin the spindle in the chamber. After five minutes of rotating, three viscosity measurements will be taken in one-minute intervals. Based on the specification, the torque should be within 10 to 98% of the motor capacity. So, the rotational speed and the spindle should be selected such that this requirement would be met. As Figure 2-10 shows, a semi-log sale plot of viscosity from RV test versus temperature can be used to determine the mixing and compacting temperatures when fabricating the asphalt mixture.

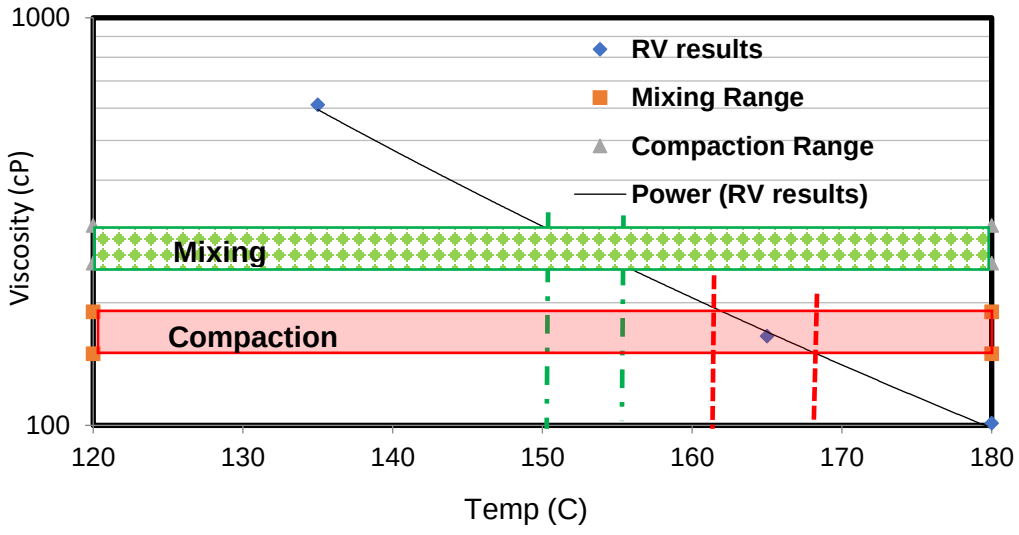

Figure 2-10. A typical Viscosity Vs. Temperature of binders

2.3.3. Dynamic Shear Rheometer (DSR)

The determination of the high temperature of Superpave performance grade (PG) requires performing tests at a wide range of medium to high temperatures. The dynamic shear modulus (G^*) and phase angle (d) are the output of the DSR test used to characterize the viscoelastic and viscous rheological properties of binders. The complex shear modulus (G*) is a ratio of the applied shear strain to the resulting shear stress. The phase angle (d) provides a relative indication of the viscous and elastic behavior of the asphalt binder. Materials with a phase angle of 90 degrees are completely viscous; while materials with a phase angle of 0 degrees are completely elastic. Regarding the rutting distress, a binder should be stiff and behave as elastic, whereas; for fatigue cracking, more flexibility and fluidity is preferred. Using the results of the DSR test, the places where a specific binder can be used to resist the temperature conditions will be determined. To perform this test, the SmartPave 102 Anton Paar DSR machine in MAPIL (shown in Figure 2-11) is applied to calculate G*/sin(d) and G*sin(d) parameters. SmartPave 102 is ideal for the most demanding measurements. It is used in the research and development of asphalt and bitumen. The machine is capable to test at a wide range of temperature from -40 to 200 ℃.

Figure 2-11. SmartPave 102 Anton Paar DSR machine in MAPIL

An asphalt sample is sandwiched between an oscillating spindle and the fixed base conditioned according to ASTM D 7175-15. The proper specimen thickness is achieved by adjusting the gap between the spindle and the fixed plate. This gap must be set before mounting the asphalt sample but while the spindle and base plate is mounted in the rheometer and at the test temperature. The thickness of the gap used depends on the test temperature and the aged condition of the asphalt. Unaged and RTFO aged asphalt, tested at high temperatures of 46°C or greater, require a small gap of 1000 microns (1 mm). PAV aged asphalts, tested at intermediate test temperatures, in the range of 4° to 40°C, require a larger gap of 2000 microns (2 mm). Likewise, two spindle diameters are used. High temperature tests require a large spindle (25 mm), and intermediate test temperatures require a small spindle (8 mm). The Superpave specifications require the oscillation speed to be 10 radians/second, which is approximately 1.59 Hz. The operator enters the value of applied stress that will cause an approximate amount of shear strain (sometimes called "strain amplitude") in the asphalt. Shear strain values vary from one to 12 percent and depend on the stiffness of the binder being tested. Relatively soft materials tested at high temperatures, (e.g., unaged binders and RTFO aged binders) are tested at strain values of approximately ten to twelve percent. Hard materials (e.g., PAV residues tested at intermediate temperatures) are tested at strain values of about one percent. To begin the test, the sample is first conditioned by loading the specimen for 10 cycles. Ten additional cycles are then applied to obtain test data. The rheometer software automatically computes and reports G* and δ, which can be compared with specification requirements.

2.3.4. Bending Beam Rheometer (BBR)

To check the low temperature of PG gradation, bending beam rheometer (BBR) is used. Since the used binder PG gradation is supposed to be PG 64-22, the BBR test was performed at 10 ℃ warmer than the PG low temperature grade which is -12 ℃. BBR is used to measure the stiffness of asphalts at very low temperatures. The test uses engineering beam theory to measure the stiffness of a small asphalt beam sample under a creep load. A creep load is used to simulate the stresses that gradually build up in a pavement when the temperature drops. Two parameters are evaluated with the BBR. Creep stiffness is a measure of how the asphalt resists constant loading and them-value is a measure of how the asphalt stiffness changes as loads are applied. The BBR (shown in Figure 2-12) gets its name from the test specimen geometry and loading method used during testing. The key elements of the BBR are a loading frame, a controlled temperature fluid bath, computer control, and data acquisition system, and test specimen. The BBR uses a blunt-nosed shaft to apply a midpoint load to the asphalt beam, which is supported at two locations. A load cell is mounted on the loading shaft, which is enclosed in an air bearing to eliminate any frictional resistance when applying load. A deflection measuring transducer is affixed to the shaft to monitor deflections. Loads are applied by pneumatic pressure and regulators are provided to adjust the load applied through the loading shaft.

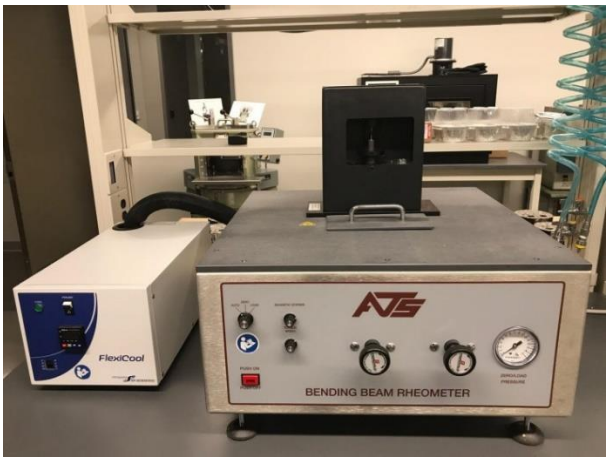

Figure 2-12. BBR test equipment at MAPIL

The bending beam rheometer is used to measure the mid-point deflection of a simply supported prismatic beam of asphalt binder subjected to a constant load applied to its mid-point. The device operates only in the loading mode; recovery measurements cannot be obtained with the bending beam rheometer. The maximum bending stress at the midpoint of the test specimen is calculated from the dimensions of the test specimen, the distance between the supports, and the load applied to the test specimen for loading times of 8.0, 15.0, 30.0, 60.0, 120.0, and 240.0 s following ASTM D 6648-01. The maximum bending strain in the test specimen is calculated from the dimensions of the test specimen and the deflection for the same loading times. The stiffness of the test specimen for the specific loading times is calculated by dividing the maximum bending stress by the maximum bending strain.

2.3.5. Multiple Stress Creep and Recovery (MSCR)

The Multiple Stress Creep and Recovery (MSCR) test method determines the percent viscoelastic strain recovery and accumulated viscoplastic strain in a binder under a predefined cyclic loading. The properties measured in the aforementioned Superpave

testing are within the linear viscoelastic region and may not fully capture the nonlinear and irrecoverable responses. The MSCR test measures parameters at higher strains, therefore, delineating binder modification strategies (e.g. polymer modification), i.e., having better potential to capture the difference between neat and modified binders in terms of rutting resistance. The test is performed per ASTM D7405-15 and measures the non-recoverable creep compliance (J_{nr}) of asphalt binders. The MSCR test is conducted using the DSR normally at the binder PGHT. The 25-mm parallel plate geometry with a 1-mm gap is used to conduct the test. In total, 30 cycles of 1 s loading and 9 s recovery are applied on the binder. The stress level in the first 20 cycles is 0.1 kPa. The first 10 cycles of 0.1 kPa loading are considered as conditioning and the measured data in the next 10 cycles followed by another 10 cycles of 3.2 kPa stress level testing are used for J_{nr} and $\%J_{nr,diff}$ parameter determination, as illustrated in Figure 2-13. Details including formulas for strain calculation are provided in ASTM 7405-15. The J_{nr} parameter is used to evaluate the rutting potential of the binder while $\%J_{nr,diff}$ determines the stress sensitivity of the tested binder.

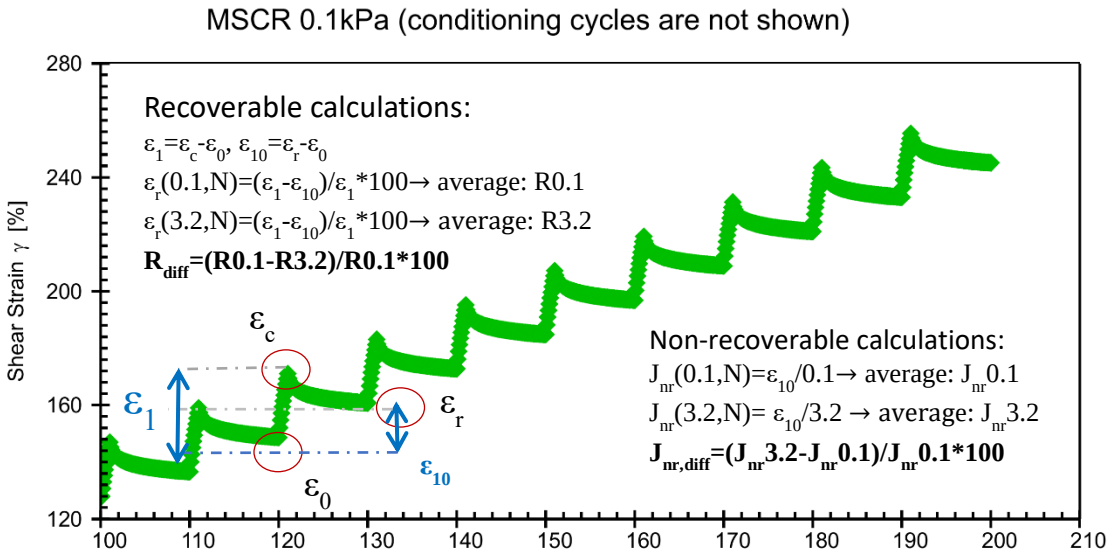

Figure 2-13. A typical strain response under MSCR test and related formulas

Following the AASHTO M-332-14, four different traffic levels are defined as S, H, V and E which stand for standard, heavy, very heavy, and extremely heavy. According to the test results, the appropriate letter is added to the PG grade of the binder.

Table 2-1 presents the Jnr and $\%J_{nr,diff}$ requirements for distinguishing different binders. For example, PG64-22 H indicates a binder suitable for heavy traffic, passing MSCR test 'H' requirements at 64 ℃ as specified in Table 2-1.

Table 2-1. MSCR thresholds

Parameter	S	H	V	E
Max Jnr, 3.2 kPa^{-1}	4.5	2	1	0.5
Max Jnr, diff %	75	75	75	75

Table 2-2 shows the RV testing results. As shown in the table, the test was carried out at two different temperatures, namely, 135 and 155 ℃. The 6 binder types which were used to run the test are neat ones. The label of the binder is the rout name in Missouri that the binder was used to prepare the mixture following by the performance grade of the binder which was reported by the plant. As an example, MO13-64-22H was used in Mo13 rout and the PG grade of this binder was labeled as 64-22 H. Comparing the viscosities obtained at two temperatures, it can be observed that as the temperature increased, the binder exhibited softer behavior and the viscosity decreased. Testing the binders at two different temperatures, provided the opportunity to define the mixing and compacting temperatures which are needed when fabricating the asphalt mixture specimens. As shown, different binders yielded different viscosities which indicate the difference in the rheological

properties of the binders at high temperatures. The various rheological properties are resulting from the difference in the chemical components of the binders. The results showed that the RV test could distinguish different binder types as the viscosity of the binders are different. For example, adding more rubber to binder makes it stiffer and harder to flow. This is completely captured by the test as the viscosity increased when the percentage of the rubber increased. This resulted in a huge difference between the mixing and compaction temperatures of the binders modified with rubber.

Table 2-2. Viscosity of binders obtained from the RV device

Binder Type	Viscosity (mPa.s)		Mixing Temp. (°C)	Compaction Temp (°C)
	135 °C	155 °C		
MO13-64-22H	653.7	261.8	165.4	153.4
US54-46-34	181.0	83.6	136.5	124.9
US63-58-28 (0% ECR)	217.2	96.4	140.7	129.3
US63-58-28 (5% ECR)	356.8	150.0	152.0	140.3
US63-58-28 (10% ECR)	475.0	222.6	162.8	148.7
US63-58-28 (12.5% ECR)	640.0	298.2	171.6	156.8

In addition to the RV test, there are other rheological tests that are normally performed to define the grade of the binders. Unlike RV, the other tests such as DSR and BBR account for the aging of the binders at different levels. Table 2-3 shows the results of the dynamic shear rheometer (DCR), and bending beam rheometer (BBR) testing which are performed on different aging levels of the binders. These tests are performed to define the performance grade (PG) of the binder following Superpave specifications. The high temperature grade

of the binder (PGHT) is determined by performing the DSR test in neat (tank) and RTFO aged binders. On the other hand, the low temperature side of the grading (PGLT) is carried out using the BBR test. This test is performed on long-term aged binders (PAV aged). The difference in both PGHT and PGLT of the binders indicates the distinction in chemical components which leads to variation in rheological properties. As shown in the table, the PGHT and PGLT of the US63-58-28 binder were very similar to those of US54-46-28. Therefore, it is expected to observe similarities in behavior under other tests. It is also worth mentioning that the other binders showed different PGLT and PGHT.

Table 2-4 shows the MSCR test result performed on some of the binders. This test is normally performed along with the PG grading tests to evaluate the viscoelastic and viscoelastic performance of asphalt binders at high temperatures. Referring to the criteria presented in Table 2-1, the letter which describes the traffic lever that can be carried was assigned. As an example, Mo13-64-22H binder can be suitable for the high level of traffic at 64 ℃. US63-58-28 binder type could not pass the criteria of MSCR testing at 58℃. Therefore, considering the MSCR test, the label of this binder needed to be changed. This makes the US58-28 binder even more similar to the US46-34. Therefore, it is expected to observe similar responses in NIR scanning results.

Table 2-3. Summary of virgin binder testing results

Binder Type	High Temperature		Low Temperature			UTI* (°C)
	Continuous PGHT	PGHT	Continuous PGLT	PGLT	ΔTc	
MO13-64-22H	70.7	70.0	-21.2	-16.0	-8.6	91.9
US54-46-34	52.7	52.0	-33.7	-28.0	-2.5	86.4
US63-58-28	56.1	52.0	-29.0	-28.0	-3.9	85.1
US63-58-28 (5% ECR)	61.2	58.0	NA*	NA	NA	NA
US63-58-28 (10% ECR)	62.6	58.0	NA	NA	NA	NA
US63-58-28 (12.5% ECR)	65.3	64.0	NA	NA	NA	NA

NA: Not available

Table 2-4. Summary of MSCR testing results

Binder	Testing Temp	Jnr, 3.2 kPa-1	Jnr, diff %	Traffic
MO13-64-22H	64	1.42	34.97	H
	70	3.49	38.36	S
US54-46-34	46	1.37	14.78	H
	52	3.62	14.78	S
US63-58-28	52	2.30	14.38	S
	58	5.52	15.01	Failed

2.3.6. List of Specifications Used for Binder Testing

As mentioned before, each binder test was performed based on a specific standard. The specifications followed in this research are listed as follows.

- ASTM D6373–16: Standard Specification for Performance Graded Asphalt Binder
- ASTM D4402–06: Standard Test Method for Viscosity Determination of Asphalt at Elevated Temperature Using a Rotational Viscometer (RV)
- ASTM D7175 – 15: Standard Test Method for Determining the Rheological Properties of Asphalt Binder Using a Dynamic Shear Rheometer (DSR)
- ASTM D6648 – 01: Standard Test Method for Determining the Flexural Creep Stiffness of Asphalt Binder Using the Bending Beam Rheometer (BBR).
- ASTM D2872 – 12: Standard Test Method for Effect of Heat and Air on a Moving Film of Asphalt (Rolling Thin-Film Oven test) (RTFO)
- ASTM D6521–13: Standard Practice for Accelerated Aging of Asphalt Binder Using a Pressurized Aging Vessel (PAV)
- ASTM D7405-15: Standard Test Method for Multiple Stress Creep and Recovery (MSCR) of Asphalt Binder Using a Dynamic Shear Rheometer

2.4. Asphalt Mixture Sample Fabrication

The asphalt materials used to fabricate the gyratory samples were collected from Illinois, Tollway project. The main goal of the sample collection was to develop a performance specification for the mixtures that were produced to pave the Tollway sections. The asphalt mixtures investigation of this project was done as a side study, after making the testing

samples and before breaking them under asphalt performance tests such as disk-shaped compact tension test (DC(T)). The asphalt materials were collected from different asphalt plants in Illinois. After being produced in the plants, the asphalt materials were collected into steel buckets and were transformed to MAPIL lab. Figure 2-14 shows some examples of the asphalt mixtures sampling from different asphalt plants. The mixture sampling included a variety of different types of asphalt in terms of binder type, aggregate type and gradation, amount of recycling materials, and asphalt binder modifier. Among a wide variety of the sampled mixtures, seven mixtures types were chosen to perform the scanning. Table 2-5 shows the specification of the seven tested mixture types. As it can be seen in the table, the asphalt mixtures had dense graded and stone matrix asphalt (SMA) types. The binder used in these mixtures had a wide variety from unmodified (neat) to modified binder types such as styrene-butadiene-styrene (SBS), ground tire rubber (GTR) and engineered crumbed rubber (ECR). In addition, the mixtures had different content of reclaimed asphalt pavement (RAP) and recycled asphalt shingles (RAS) as the recycled pavement materials. The ABR by RAP ranges from 11 to 27% while the range of ABR by RAS is 10 to 18%. The RAP and RAS content are identified by the asphalt binder replacement which is defined as the proportion of the binder which is obtained to be reused with respect to the binder needed to make the mixture such that it meets the volumetric requirements. In addition, each mix used an additive which is either warm mix or antistripping agent to boost the performance of asphalt concrete and make it more resistant to cracking and moisture damage.

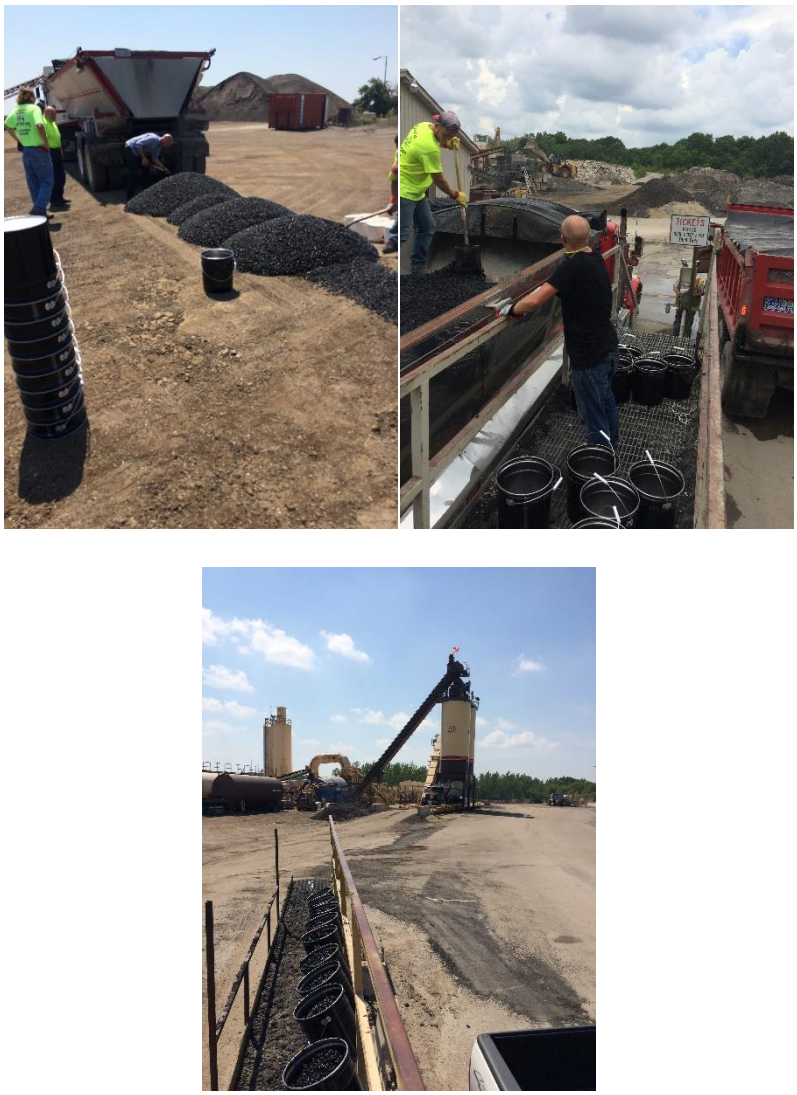

Figure 2-14. Sampling asphalt materials from different plants in Illinois

Table 2-5. Specification of the asphalt mixture types

	Mix. No	Label	Neat Binder	ABR by RAP	ABR by RAS	Additive
Dense	1	1823	SBS 64-34	24.1	14.2	0.4% Evotherm P26
Graded	2	1826	46-34	27.6	18.1	0.4% Evotherm
	3	1824	SBS 64-34	20.4	16.7	0.4% Evotherm P25
	4	1835	46-34+10%ECR	25.5	16.1	0.4% Evotherm J12
SMA	5	1836	SBS 64-34	16.2	16.3	0.4% Evotherm J12
	6	1840	58-28+12GTR	15.9	9.8	0.4% Ingevity J1
	7	1844	SBS 70-28	10.8	16.0	0.4% Ingevity J1

The aggregate gradation of the studied mixture types is shown in Figure 2-15. The gradation of the aggregate is normally presented in a semi-log chart in which the vertical axes is the passing percentage of aggregate by weight in arithmetic scale and the vertical axes are the sieve size in mm in log scale. As it can be seen, the dense graded mixtures (1823 and 1826) are completely distinguishable from the SMS mixtures. As its aggregate gradation curve is placed above the other mixtures, the 1823 mix with a nominal maximum aggregate size of 4.75 mm has the finest (smallest) aggregate structure. The other dense graded mixture (1826) has an NMAS of 9.5 mm and is relatively coarser than 1823. The SMA mixtures had almost the identical aggregate gradation with all the NMASs equal to 12.5 mm. From Table 2-5 and Figure 2-15, it can be inferred that the collected asphalt materials differed from each other. This verity provided the opportunity to collect a decent dataset which was used to make analysis and comparisons.

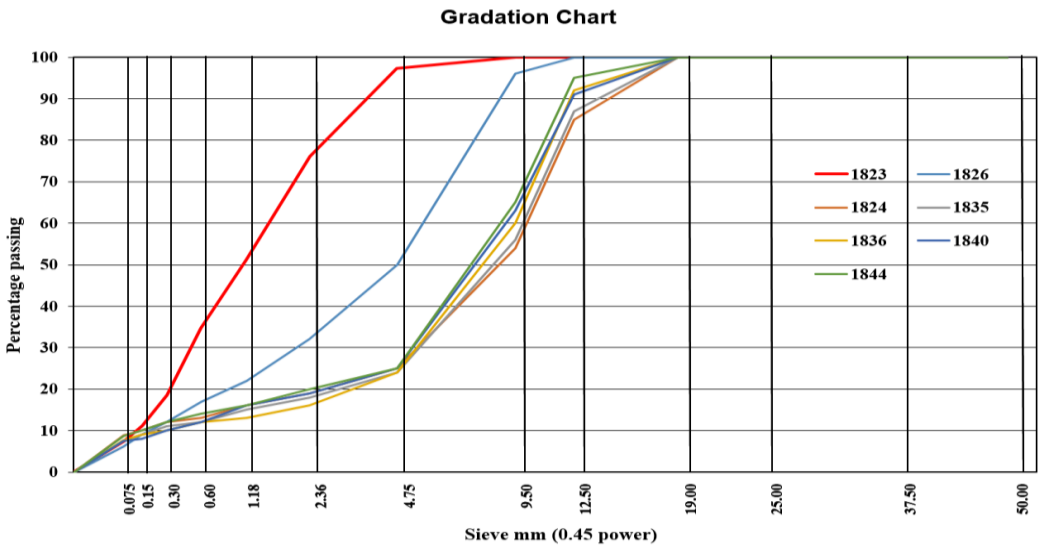

Figure 2-15. Aggregate gradation of the mixtures

A gyratory compactor machine in MAPIL lab was used to fabricate gyratory samples. To this end, the buckets containing the asphalt mixtures were heated up in the oven to the point (normally 110±10 ℃) that they could be easily split into pans. In order to perform the performance test, cylindrical samples of different height needed to be made. Based on the volume of the testing samples, different masses of asphalt mixtures were put into the gyratory mold to fabricate cylindrical specimens (Figure 2-16).

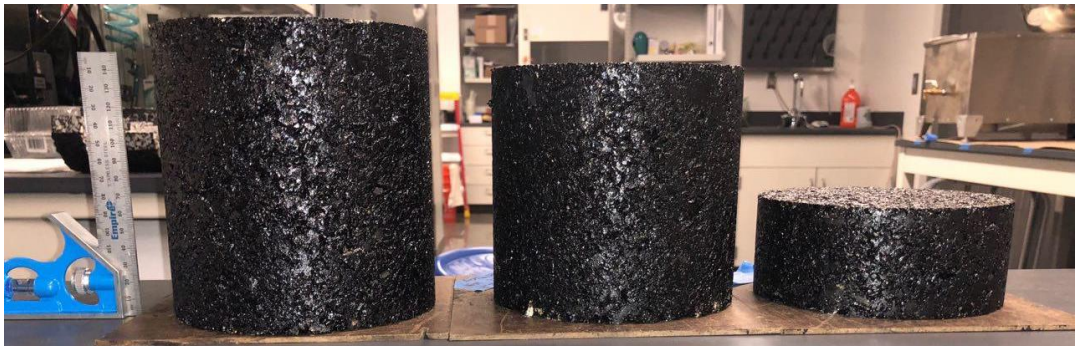

Figure 2-16. Asphalt specimen preparation

CHAPTER 3.

THE NIR MICRO SPECTROMETER FOR ASPHALT BINDER CHARACTERIZATION

3.1. Binder Characterization Using the NIR Micro Spectrometer

Asphalt material contains two major parts: the aggregates and the binder. The binder is the black liquid part, which functions as a glue to hold the aggregates together. The binder can be modified with different materials such as rubber, rejuvenator, and recycled binder. This component has a very important role in asphalt performance and characterization. The latest method of asphalt binder grading (Performance Grading (PG)) defines criteria to assure the performance. Then, the binder is classified based on the highest and the lowest temperatures that it can meet those criteria. In this section, binders with different PG classifications are studied using the SCiO NIR sensor.

3.2. Scanning process

In order to scan the binder using the SCiO sensor, it was placed in a mold which was compatible with the geometry of the sensor. This way, the SCiO sensor could be placed on the edges of the mold to scan a binder. Figure 3-1 presents the fabricated mold. As seen, the idea behind the configuration and shape of the mold is coming from the BBR sample molds. The same metallic pieces were put together to make a shallow rectangular-like container to contain the binder. The difference between the molds is that the designed one has larger width such that the sensor can seat on it. Also, the dividers were used to provide

further support for the sensor which seats on the mold. In addition, the dividers could provide the opportunity to have three binder types in one mold.

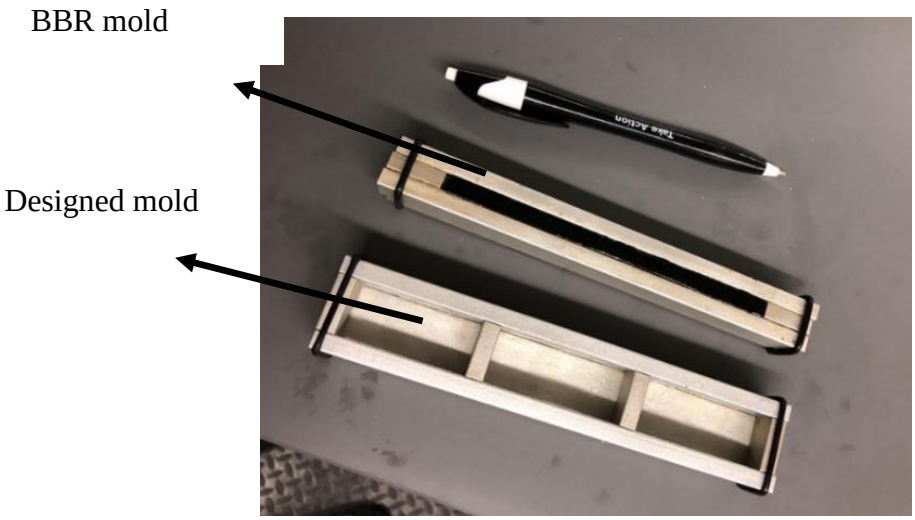

Figure 3-1. Comparing the designed and the BBR molds

3.3. Binder Characterization Results

A number of binders with varied PG grades, rubber percentages, and aging levels were scanned and analyzed. The neat binder represents a non-aged status. The second level is the RTFO. The RTFO samples represent binders that are aged via exposing to heat and pressure and being mixed with aggregate in an asphalt plant. These samples are ready to be placed on the road surface. The third level is PAV aged samples which represent the aging that the binder has experienced after being about 7 to 10 years under service. Also, the rubber modified binders contain a wide range of rubber dosage from 0 to 12.5% by mass of the binder. A series of the plots are provided to make a comprehensive comparison between the responses and study the efficiency of NIR in distinguishing different binder

types. The plots show the average of the first derivative of the log of raw data (later referred to as processed data) in a range of 740 to 1040 nm of wavelength.

Figure 3-2 shows the results for the PG 46-34 binder at 3 different aging levels. While the RTFO binder response is bumpy, the neat and PAV binders have a smoother trend. The RTFO-aged binder has the most distinct response especially in the wavelength range of 800 to 880 nm compared to the neat binder and PAV-aged binder. The PAV-aged binder has similar trends to the neat binder. The main difference between the responses of neat and PAV binders is in the first part of the graph (wavelength of 740 to 770 nm) where the PAV has an upward trend while the response of the neat binder has a decreasing trend.

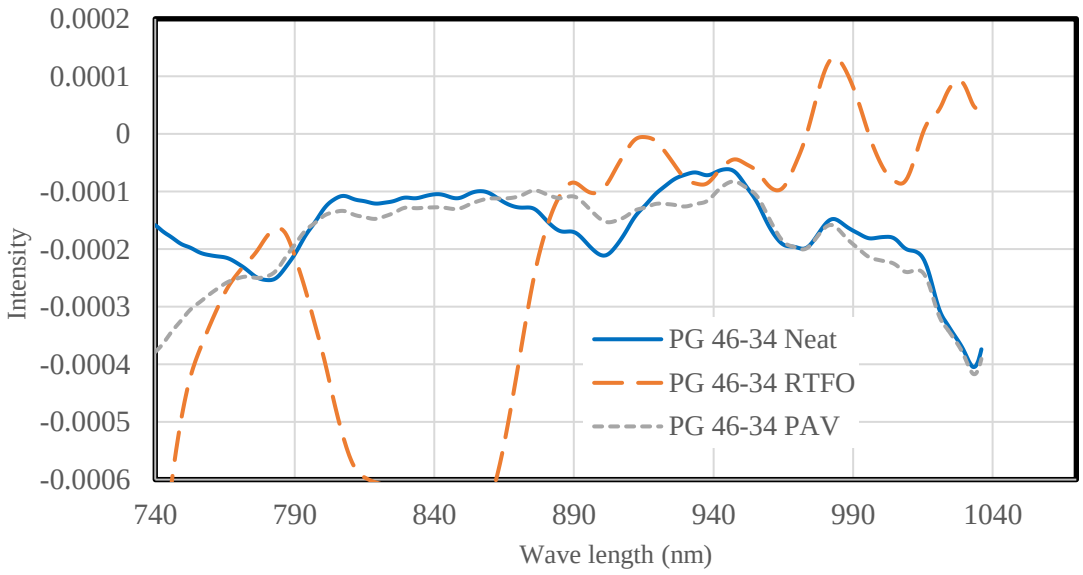

Figure 3-2. Comparison of the PG 46-34 binders with different aging levels

Figure 3-3 shows the processed response for three different aging levels of the PG58-28 binder. As shown in this figure, the binders followed different patterns and levels of response at the beginning of the wavelength and then became closer to each other as the

wavelength increases. The wavelength of 800 to 880 nm is the range that these binders showed the most distinguishable responses. The neat binder had the highest values in this range while the intensities of the PAV and RTFO-aged were lower than the neat binder. The RTFO binder showed the highest variability in the studied wavelength while the neat and the RTFO binders had relatively gentle slopes on their response curve. After the wavelength of 890 nm, all the three binders started to follow a more similar trend. Therefore, this range of wavelength can also be a potential candidate for classification proposes for the tested PG58-28 binder.

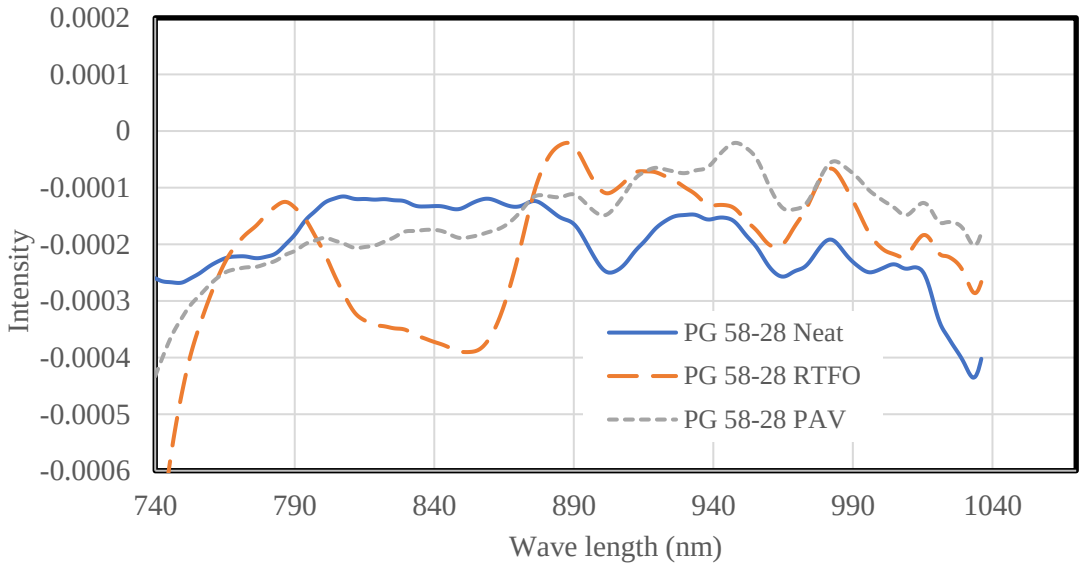

Figure 3-3. Comparison of the PG 58-28 binders with different aging levels

Figure 3-4 shows the PG 58-28 binder modified with 5% rubber. Compared to the PG58-28 binder with 0% rubber, this binder showed even more distinguishable response in 800 to 880 nm of wavelength range. In additions, the responses of 5% binder modified have more peaks, where the first derivative of the processed response is zero. Again, the same pattern observed in the previous figures is seen here as the RTFO-aged binder has a sudden

drop and then increase in 800 to 880 nm. The neat and PAV-aged binders follow almost the same pattern but with differences in periods such as 740 to 800 nm and 900 to 950 nm. The added 5% rubber in the binder led to more distinct differences, especially for the RTFO binder. The neat binder has the highest peak at 980 nm; whereas the RTFO graph has peaks around 780, 880, and 920 nm. At the beginning of graphs, the RTFO graph starts with lower values in comparison to the other two binders. For wavelengths larger than 920 nm, RTFO has a higher intensity than the neat and PAV-aged binders.

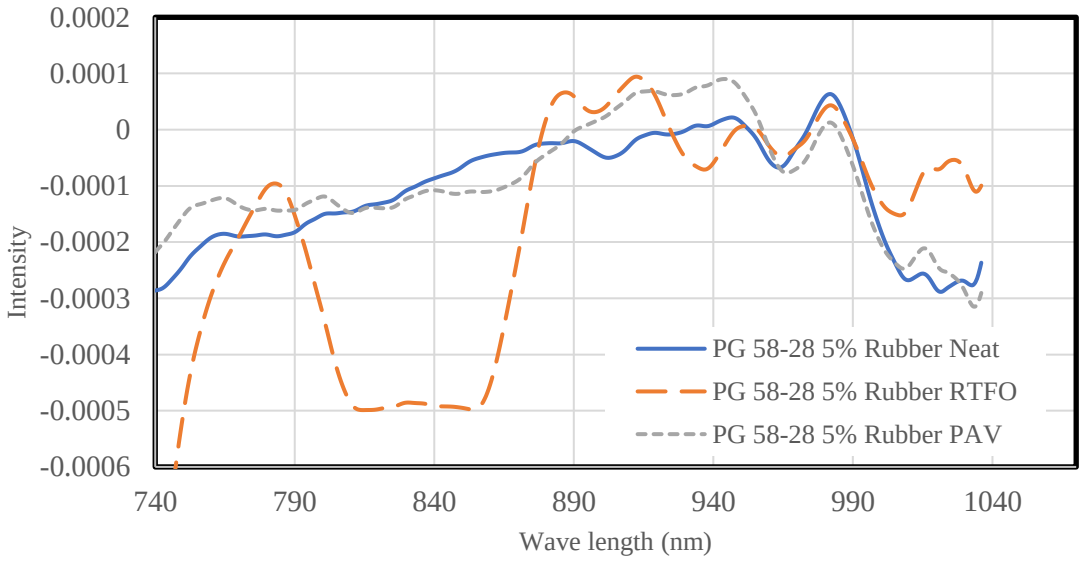

Figure 3-4. Comparison of the PG 58-28 binders with 5% rubber at different aging levels

Figure 3-5 shows the PG 58-28 binder with 10% rubber at 3 different aging levels. Unlike the other binders studied before, the trends are very similar for all the aging levels. The responses followed an upward trend from the beginning to a wavelength of about 900 nm. After that, the intensities decrease at a similar rate. One of the differences between the responses of the aging levels is the wavelength that gives peak intensities. In terms of the

magnitude of the response, the previously captured wavelength range of 800 to 890 is a suitable one to detect the differences; however, the trend is similar in this range. As shown, the highest peak of neat binder occurred earlier compared to the other two aged binders. Surprisingly, both the rate and the values if the processed response is identical in the wavelength range of 970 to 1020 nm. It appears that adding more than 5% rubber has changed the trend in the binder responses at different aging levels. Further rheological testing might also capture this similarity in the behavior of the PG58-28 binder modified with 10% rubber.

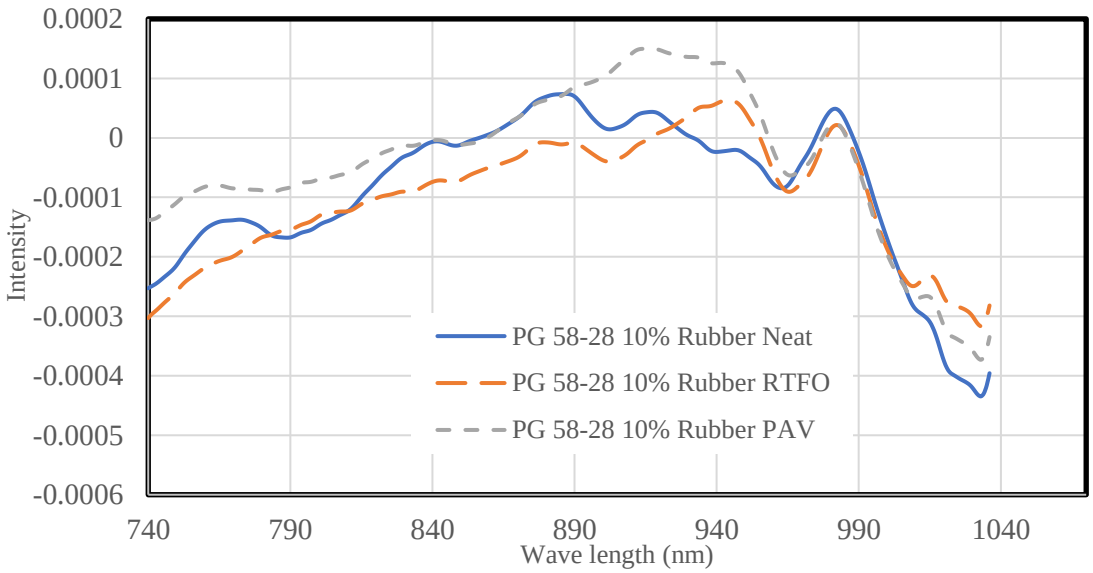

Figure 3-5. Comparison of the PG 58-28 binders with 10% rubber at different aging levels

Figure 3-6 shows the responses of the PG 58-28 binder modified with 12.5 % rubber at different aging levels. Similar to 10% rubber modified binders, these binders did not exhibit very distinguishable responses. This similar behavior between different levels of aging started to be observed when 10% rubber has been added to binders and continued for 12.5%

rubber. Again, more rheological testing on these two binders may verify this observation. It appears that the addition of rubber more than 5% does not significantly change the chemical components of the binders after they are aged at different aging levels. That being said, the number of peaks and also the response values in the 800 to 890 can help with the discrimination of the binders. As shown in the figure, the neat binder is less bumpy than the other two aged binders.

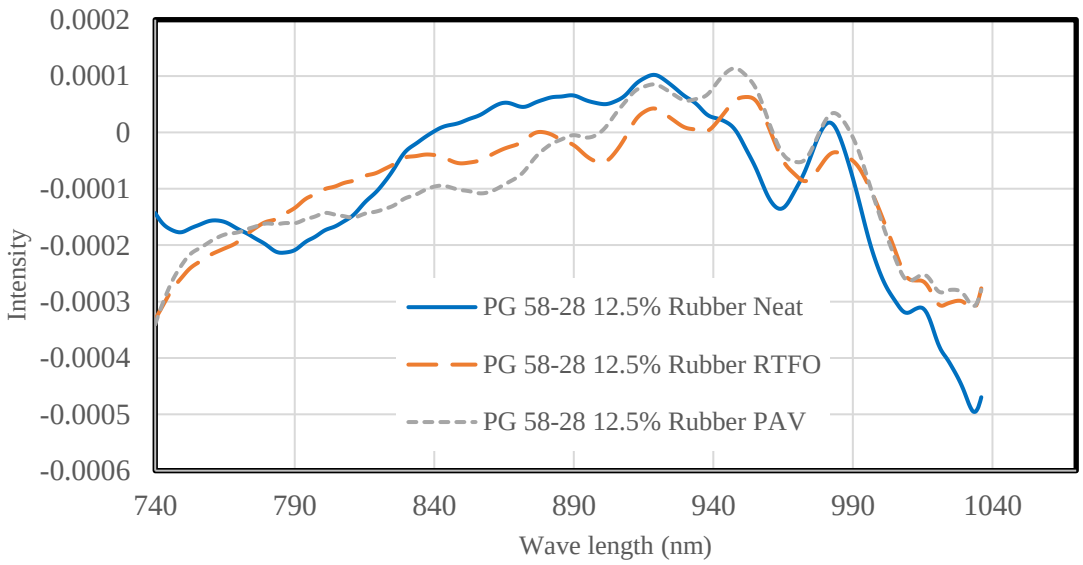

Figure 3-6. Comparison of the PG 58-28 binders with 12.5% rubber at different aging levels

Figure 3-7 to Figure 3-12 present the comparison of the same levels of binder but different performance grades or percentages of rubber. As shown in these figures, the spectrum of the binders varies in different cases such as the magnitude of response and also the trend over the studied wavelength. As an example, Figure 3-10 shows the results for four different percentages (0, 5, 10, and 12.5%) of rubber content. As the lowest difference between the contents is 2.5% (10 and 12.5%), it was expected to observe the lowest difference between the spectrum of10 and 12.5% rubber contents. As shown in the figure,

they show similar trends and values within the studied wavelength. The binder with 12.5% rubber has a peak at 920 nm, and it has the lowest value in comparison to others at the end of 1040 nm. The neat binder has the lowest value in a wide area from 840 to 1000 nm in comparison to other graphs. PG 58-28 binder with 5% rubber content has the highest value in comparison to other 3 graphs at the end of 1040 nm and it has a peak at 880 nm. The ability to detect the parameters considered in this study (aging, grade, and rubber percentage) could provide the user with a tool to detect different binders studied in this project.

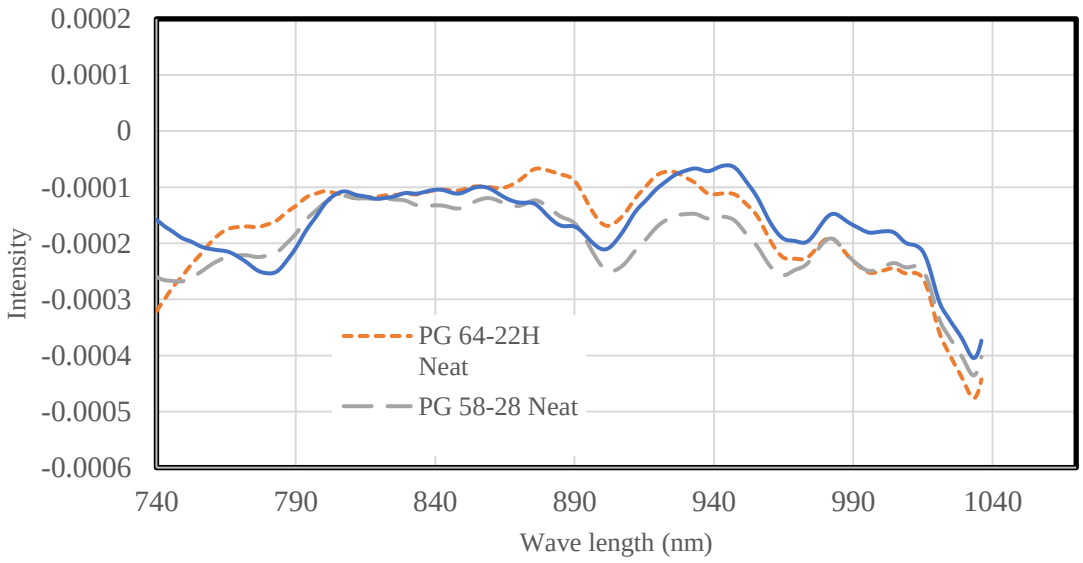

Figure 3-7. Comparison of different neat binders

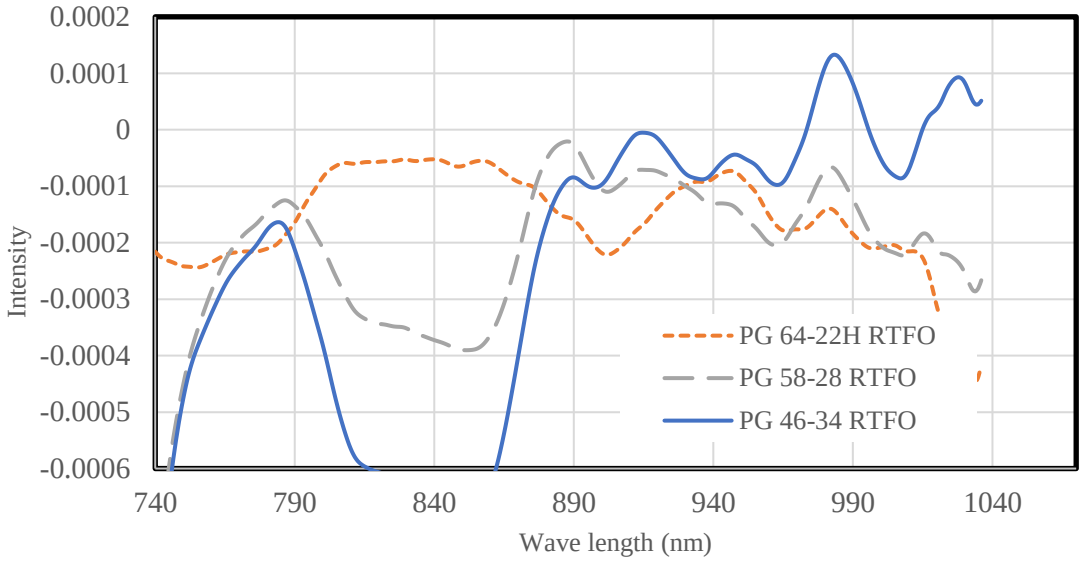

Figure 3-8. Comparison of different RTFO-aged binders

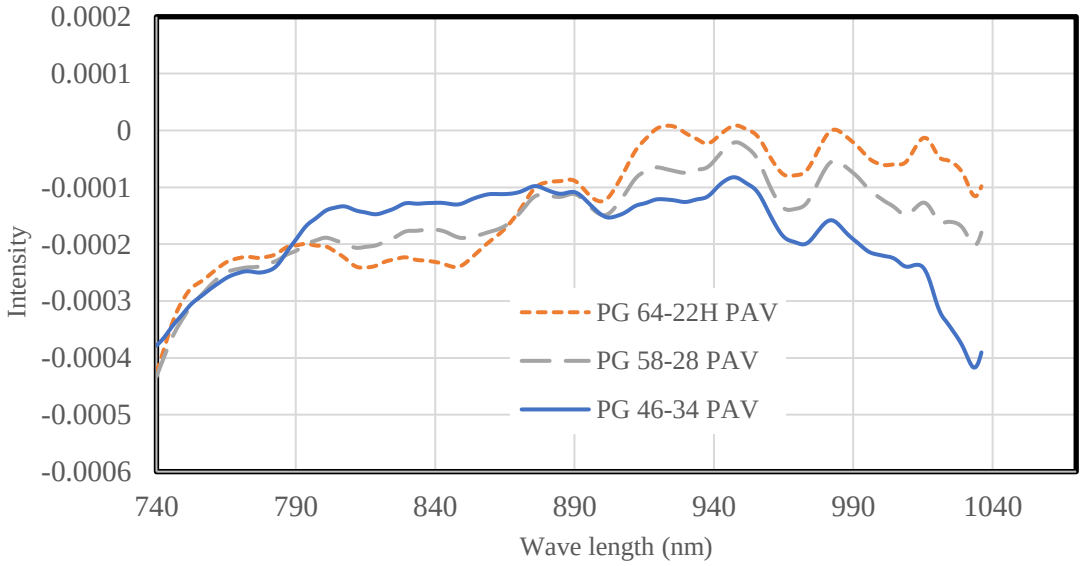

Figure 3-9. Comparison of different PAV-aged binders

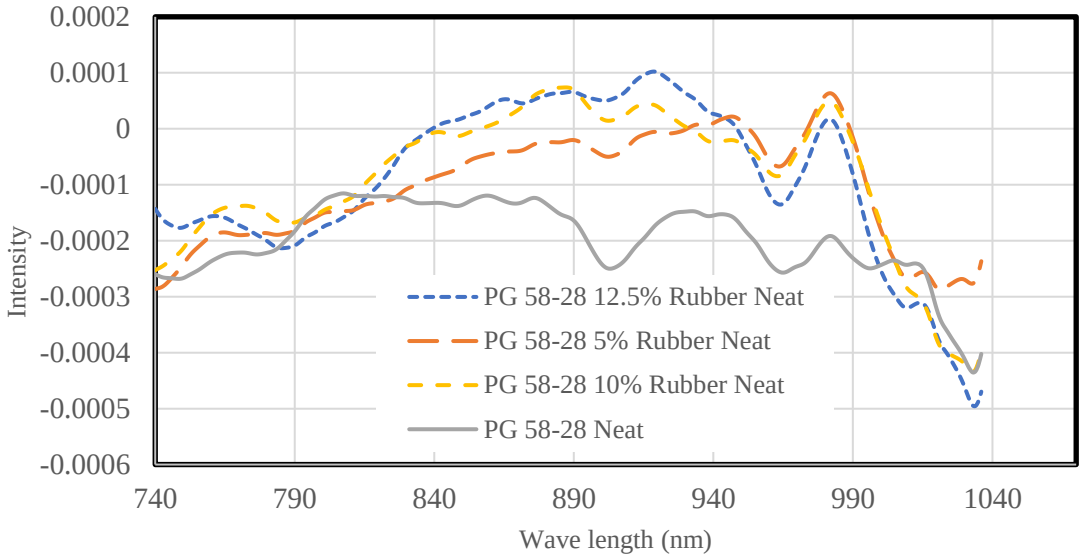

Figure 3-10. Comparison of the PG 58-28 neat binders with different percentage of rubber

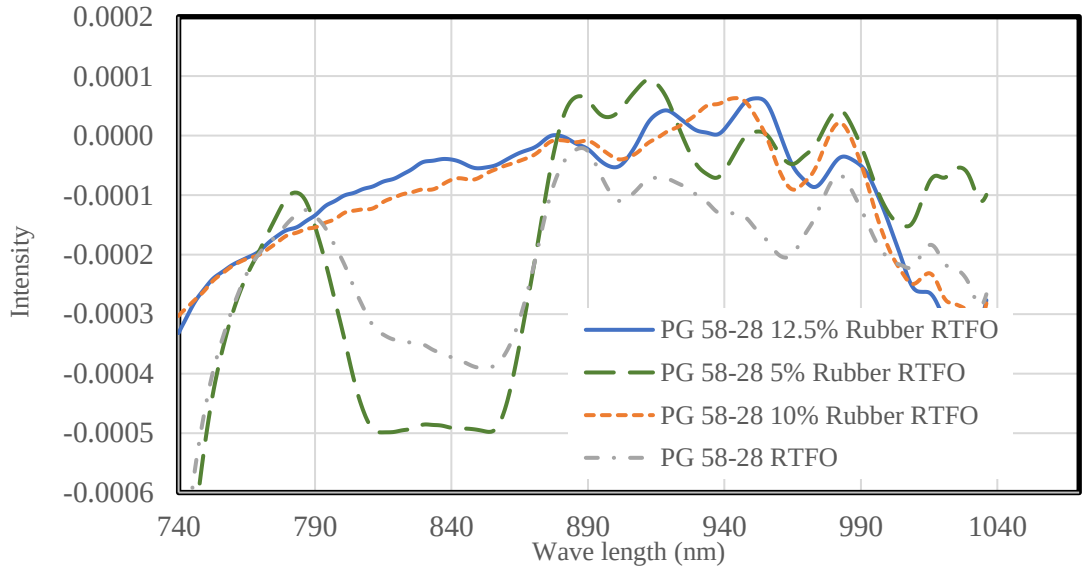

Figure 3-11. Comparison of the PG 58-28 RTFO binders with different percentage of rubber

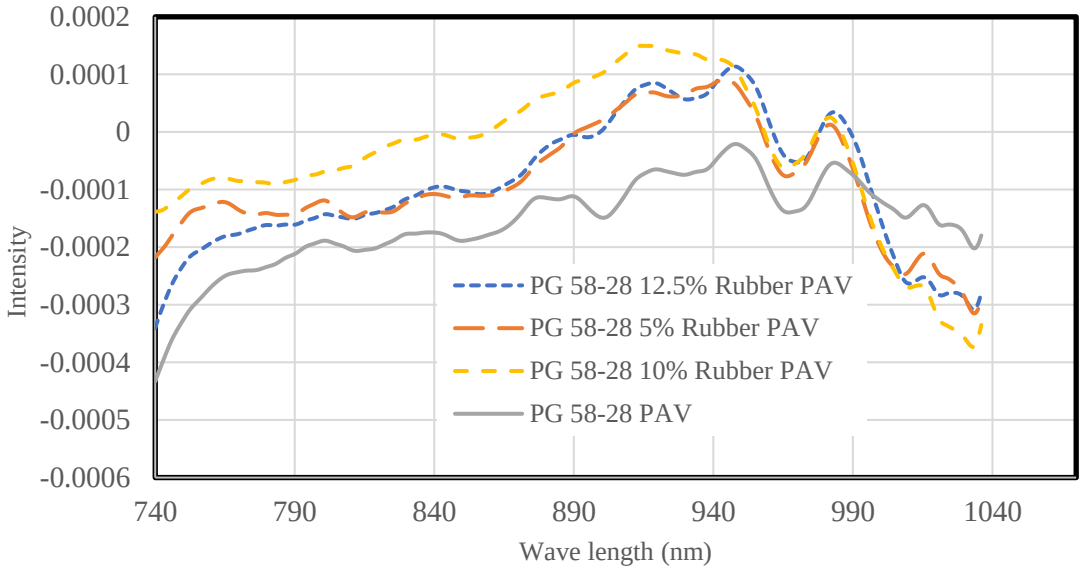

Figure 3-12. Comparison of the PG 58-28 PAV binders with different percentage of rubber

CHAPTER 4.

THE NIR MICRO SPECTROMETER FOR ASPHALT MIXTURE CHARACTERIZATION

4.1. Mixture Characterization Using the NIR Micro Spectrometer

Figure 4-1 shows some of the gyratory specimens which were compacted using the asphalt materials collected at different asphalt plants in Illinois. After compaction, the samples are normally still hot and may deform easily. Therefore, the gyratory compacted samples were kept in front of a fan to cool down overnight. These samples were 15 cm (6 in) in diameter and 95 mm (3.75 in) in height. Two different aggregate structures, namely, dense graded and SMA, made the gyratory specimens look different such that the SMA specimens did not have a smooth surface as this aggregate structure does not contain the aggregates in the middle range of sieve sizes. As a result, the surface looks porous. On the other hand, the dense graded specimens have more evenly distribution of aggregates passing through the sieves. Another aggregate feature that made the seven tested mixtures distinct is the NMAS, such that the SMA mixtures had larger aggregates compared to the dense graded mixtures. The differences in the aggregate properties were expected to result in a different spectrum of responses between SMA and dense graded specimens.

Another parameter which was proven to have effects on the scan results was the type of the binder which could be modified by rubber. In the set of the tested mixtures, the binder types within the mixtures were miscellaneous and included unmodified, polymer modified (SBS), and rubber modified (ECR and GTR). Therefore, the sensor response can be

dependent on the type of the binder that coated the aggregates as well as the structure of the aggregates.

Figure 4-1. Asphalt mixture samples in MAPIL

For a better replication, the Autodesk 360 software was used to design a 3D printed mold with the dimension of the sensor. The netted 3D printed mold with 10 empty cells shown in Figure 4-2. The mold perfectly fitted the mixtures samples and provided the opportunity to scan the surface at different locations. The dimension of each empty cell of the mold is 42 by 21 mm which is the exact same dimension of the SCiO sensor. The surface of the specimens was scanned once through each cell and the results were transferred to the cloud to be processed. Similar to the binder spectrums, the responses were plotted after taking the first derivative of the log of the raw data.

Figure 4-2. The 3D printed mold used for scanning asphalt mixture samples

4.2. Asphalt Mixture Characterization Results

Asphalt Mixtures contain both binder and aggregate. This makes the data interpretation more complicated because the scanned spectrum includes the integrated response of the aggregates and binder. Therefore, each of the available six samples was scanned 30 times. The average of the 30 scans was then reported herein.

4.2.1. Detecting Dense Graded Mixture Containing SBS Polymer (Mix 1823)

Mix # 1823 is a dense graded mixture with a PG 64-34 binder modified by SBS polymer. In addition, it has 24.1% ABR by RAP as well as 14.2% ABR by RAS. The NMAS of this mixture is 4.75 mm. Figure 4-3 shows the spectrum of this mixture which was processed

by applying the 1st derivative with a 35 window on the log of the raw data. Similar to the binder responses, the corresponding spectrum for this mixture also followed an increasing trend in a wavelength range of 740 to 890 and then started decreasing. This observation can be justified by the fact that the aggregates in an asphalt mixture are coated with the binder, and binder is the first material which receives the illumination from the sensor. Afterward, this illumination is sent back through the binder. Therefore, the binder is expected to play a significant role in the response of the material. That being said, comparing to the binder plots, this mixture had a completely different range of response. In order to perform a fair comparison, all the mixtures in this section were plotted from -0.0002 to 0.0016 on the y-axis while the binder response plotted in a range of -0.0006 to 0.0002. It was observed that the aggregates made the response of the mixture distinct from the binder.

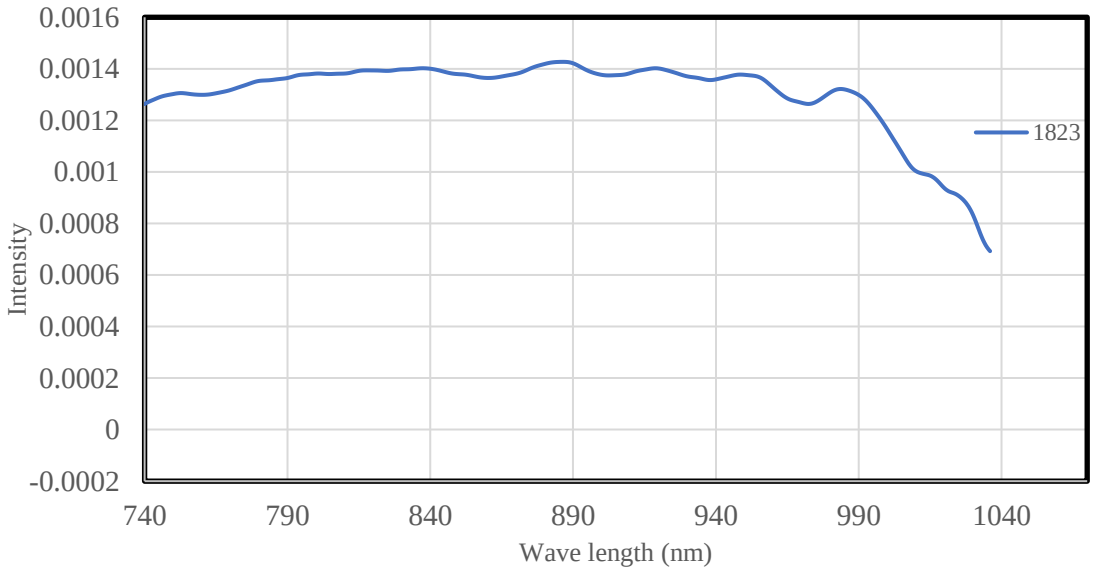

Figure 4-3. Analyzed spectrum of mix # 1823

4.1.2. A Comparative Study between Dense Graded Mixtures 1823 and 1826

Figure 4-4 compares the response of mix # 1823 with the fingerprint spectrum of mix # 1826. Mix # 1826 is a dense graded and the neat binder used in this mixture is 46-34 which has not been modified by polymers and rubber. Mix # 1826 has 27.6 %ABR by RAP and 18.1% ABR by RAS. The same process of the 1st derivative was done on this graph to calculate the processed response. Compared to mix # 1823, 1826 mixture started the spectrum at a value of around 0.0007. Until the wavelength of 940 nm, the two dense graded mixtures were completely distinguishable. The difference in the response can be attributed to both aggregates and binders. However, the difference between these two mixtures could not be captured by the sensor as their response was very similar to each other.

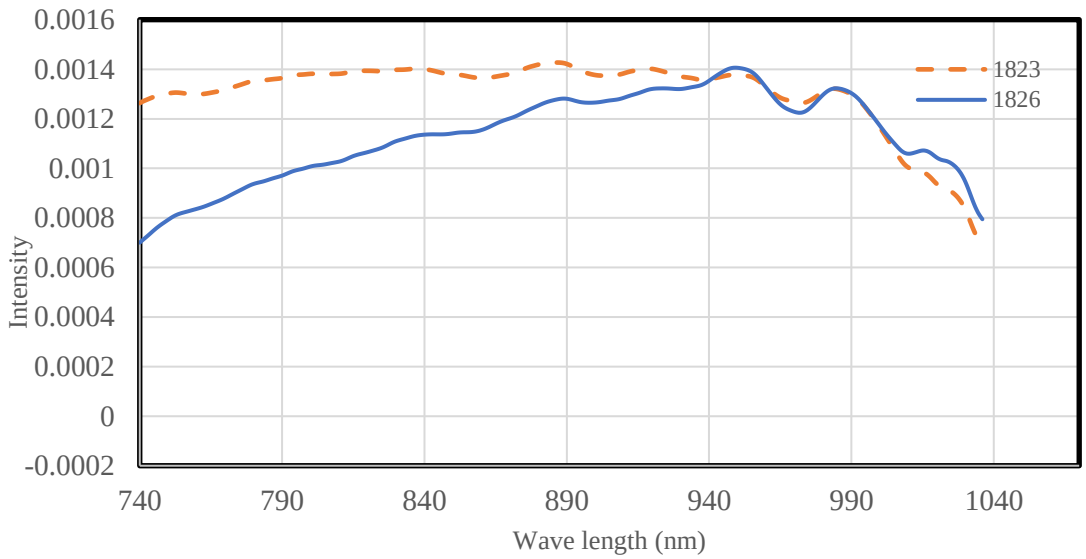

Figure 4-4. Comparing two dense graded mixtures (mixes # 1823 and 1826)

4.2.3. A Comparative Study between the SMA Mixtures with SBS Modified Binder

As mentioned in Table 2-5, there were three SMAs in the mixture list that are all modified with SBS polymer, namely, 1824, 1836, and 1844. Also, as shown in Figure 2-15, the aggregate structure is very similar in these three mixtures as they are all SMAs. However, these three mixtures are different in terms of the source of the aggregates and binder, type of additive, and also the percentage of recycled materials. As shown in Figure 4-5, mix # 1844 yielded the lowest spectrum between the three mixtures. It means that the intensity of the reflected illumination from the surface of mix # 1844 had the lowest rate comparing to the other two samples. In this respect, mixes # 1836 and 1824 had the first and second place in terms of the processed response magnitude. Again, the trend observed in the response of all the mixtures are similar and the only difference is the value of the 1^{st} derivative (rate) of intensity. As observed before, the difference between the mixture response and binder response is the range of the 1^{st} derivative (processes raw data), while the trend of asphalt materials (either asphalt binder or asphalt mixture) is basically identical. Figure 4-5, shows that the application of NIR via the smartphone-based sensor could detect different mixtures that were similar in terms of aggregate structure and binder modifier.

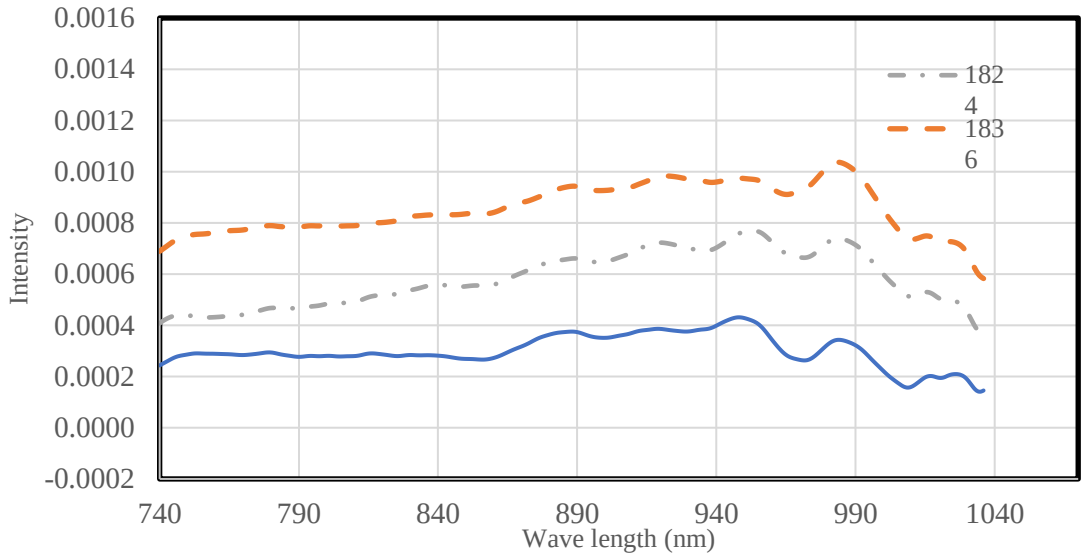

Figure 4-5. Comparing three SMA mixtures modified with SBS

4.2.4. A Comparative Study between SMA Mixtures with Rubber Modified Binder

In this part, the two SMA mixtures (# 1835 and 1840) with rubber modified binders were compared together. Mix # 1835 contained engineering crumb rubber (ECR) while mix # 1840 had typical ground tire rubber (GTR). Referring back to Figure 2-15 and Table 2-5, the neat binder, amount of recycled materials, and also the additive types are different in these two mixtures. Therefore, it is expected to observe distinct processed responses in these two mixtures. The responses of the scans captured by the SCiO sensor are plotted in Figure 4-6. As shown, the ECR modified mix had a higher change of reflection rate from the surface compared to 1840 mixture with GTR. The trend of the 1st derivative did not change compared to other mixtures and an increasing trend was observed in the processed response till wavelength of around 940 nm and then it followed a decreasing trend. In general, mix # 1840 had a more uniform rate of reflection throughout the studied wavelength range.

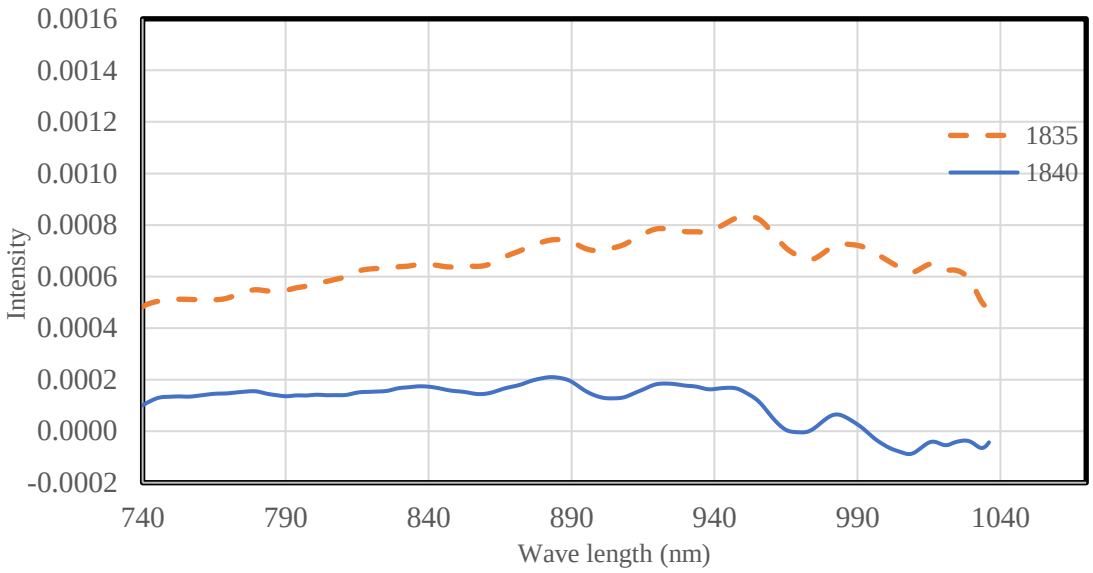

Figure 4-6. Comparing three SMA mixtures modified with rubber

4.2.5. An Inclusive Comparative Study of the Tested Mixtures

In this section, a more thorough comparison was made using the complete data set of the seven tested mixtures (see Figure 4-7). The interesting observations from this comparative study are as follows:

- The highest response belonged to a dense graded mix with SBS modified binder (# 1823) and the lowest was exhibited by mix # 1844 which is an SMA with rubber modified binder.
- All of the mixtures were following almost the same trend but have different response magnitudes. In general, the intensities were increasing from the beginning to a wavelength of around 940 nm and then started to decrease immediately after.
- Mixes # 1823 and 1826 as the dense graded mixtures exhibited distinct responses comparing to the SMAs. The top two curves can be distinguished from the other curves.

Also, as can be seen, the decreasing tale of these two responses (after wavelength of 940 nm) had higher rates.

- The interaction of SBS polymer with a lower amount of recycled materials used in mix # 1824 resulted in almost the same magnitude of processed response with mix # 1835 which had ECR modified binder with more recycled materials.

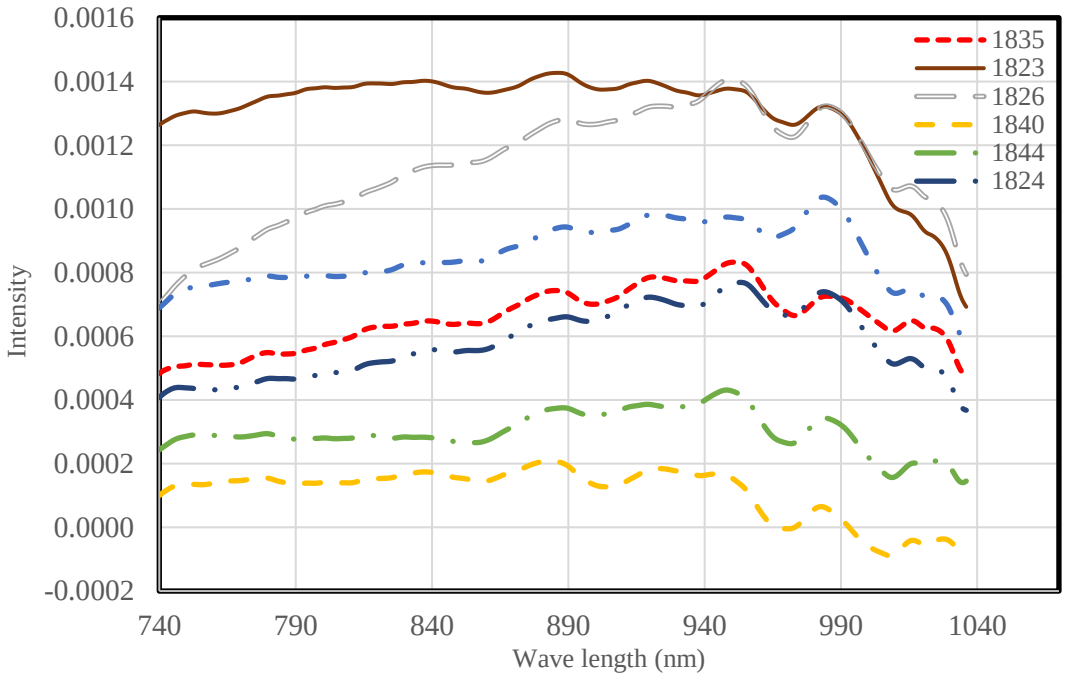

Figure 4-7. Average for raw data results for 6 different samples (30 scans per sample).

CHAPTER 5.

SUMMARY AND CONCLUSION

Asphalt pavement maintenance and rehabilitation is a time-consuming and costly process. Numerous methods have been developed for a proper and cost-effective evaluation of pavement conditions. Age-related degradation is one of the major distresses affecting asphalt pavement systems. Detection of pavement aging provide the chance to come up with timely and appropriate damage prevention strategies. In this project, the world's first pocket-sized NIR micro spectrometer was deployed for detecting asphalt binder ageing as well classifying various asphalt binder and mixture types. The NIR spectrometer has been fully integrated with the smartphone technology for real-time monitoring. The real-time material characterization analysis service provides testing results instantly via a smartphone app upon scanning of the samples. The output of the sensor is a spectrum within a wavelength range of from 740 to 1040 nm showing the intensity of the reflected illumination from the surface of the materials. In this method, the NIR spectrometer illuminates a sample with a broad-spectrum of near-infrared light, which can be absorbed, transmitted, reflected, or scattered by the sample. The light intensity is measured as a function of wavelength before and after interacting with the sample. Thereafter, the diffuse reflectance, a combination of absorbance and scattering, caused by the sample is calculated.

The portable smartphone-based NIR method was used to detect asphalt binders with various performance grading (PG) and aging levels. To magnify the differences in the response, mathematical functions such log and first derivative were applied to the raw data. Eighteen binder types with different PG grades, aging level, and rubber content were tested

under different rheological tests such as rotational viscosity (RV), dynamic shear rheometer (DSR), and bending beam rheometer (BBR). After comparing the rheological behavior of the binders using Superpave experimental tests, the binders were scanned by the sensor. The obtained results from the scans of eighteen binder types showed that the NIR sensor is capable of detecting the differences between binder types with a good accuracy using the collected data set. These distinctive spectrums can be attributed to the variations of binder components such as saturate, asphaltenic, resin, and aromatic.

Furthermore, the molecular sensor was deployed to detect and classify asphalt mixtures fabricated with a various binder and recycled material types such as styrene-butadiene-styrene (SBS), ground tire rubber (SBS), engineered crumbed rubber (ECR), reclaimed asphalt pavement (RAP), and recycled asphalt shingles (RAS). Seven asphalt mixtures collected from different asphalt plants were categorized into two major groups as dense graded and SMA graded mixtures. The difference between these two groups is the aggregate structure. Also, a wide range of binder types was used to make the asphalt mixtures including unmodified and SBS, GTR, and ECR modified binders. Similar to the binder testing results, the processed response of the mixtures under the sensor scans showed that the NIR has the capability of classifying the mixtures based on their aggregate structure and binder type.

Although the efficiency of the proposed framework is verified for some asphalt binder and mixtures, its applicability is not limited to the investigated cases. In fact, this innovate sensing systems can be modified to become a building block of future civil engineering material characterization systems. The beauty of this portable detection system is that it can be readily used by citizens for varied material characterization missions. However,

there are still some challenges that are the focus of future research. The specific effect of each parameter such as aggregate gradation, binder type, and content, modifier, and additive can be detected once the appropriate asphalt samples are fabricated. Extensive databases of the NIR spectra for a range of asphalt binders and mixtures should be developed to calibrate robust machine learning algorithm capable of detecting any type of binder and mixture. Moreover, embedded the NIR sensor inside the smartphones will make it more practical for crowdsensing purposes.

BIBLIOGRAPHY

American Society of Civil Engineers. 2017. “A Comprehensive Assessment of America’s Infrastructure.” *Asce*, 111. https://doi.org/10.1007/978-3-319-13296-9_12.

Augusto, João, Oliveira Gonçalves, and Venâncio De Carvalho. 2013. “Engenharia Civil.”

Bechadergue, Bastien, Luc Chassagne, and Hongyu Guan. 2016. “Visible Light Phase-Shift Rangefinder for Platooning Applications.” *IEEE Conference on Intelligent Transportation Systems, Proceedings, ITSC*, no. Lv: 2462–68. https://doi.org/10.1109/ITSC.2016.7795952.

Buttlar, William G., and Shahidul Islam. 2014. “098IY04 Integration of Smart-Phone-Based Pavement Roughness Data Collection Tool with Asset Management System,” 36.

Chang, T K, R J Chang, and K J Liu. 2005. “Detection of Pavement Distresses Using 3D Laser Scanning Technology.” *Computing in Civil Engineering*, no. 2005: 1–11. https://doi.org/10.1061/40794(179)103.

David H.Timm,Angela L.Priesr, Thomas V.McEwen. 2004. “Design and Instrumentation of the Structural Pavement Experiment At the NCAT Test Track.” *NCAT Report 04-01*, no. April.

Herold, M. 2004. “Understanding Spectral Characteristics of Asphalt Roads.” *National Center for Remote Sensing in Transportation (NCRST) University of California Santa Barbara (UCSB)*, no. May: 1–8.

Hou, Xiangdao, Songtao Lv, Zheng Chen, and Feipeng Xiao. 2018. “Applications of Fourier Transform Infrared Spectroscopy Technologies on Asphalt Materials.”

Measurement: Journal of the International Measurement Confederation 121 (March): 304–16. https://doi.org/10.1016/j.measurement.2018.03.001.

Huang, Yaxiong. 2006. "Automatic Inspection of Pavement Cracking Distress." *Journal of Electronic Imaging* 15 (1): 013017. https://doi.org/10.1117/1.2177650.

Jia, Xiaoyang, Baoshan Huang, Benjamin F. Bowers, and Sheng Zhao. 2014. "Infrared Spectra and Rheological Properties of Asphalt Cement Containing Waste Engine Oil Residues." *Construction and Building Materials* 50: 683–91. https://doi.org/10.1016/j.conbuildmat.2013.10.012.

Kawahara, Fred K. 1969. "Identification and Differentiation of Heavy Residual Oil and Asphalt Pollutants in Surface Waters by Comparative Ratios of Infrared Absorbances." *Environmental Science and Technology* 3 (2): 150–53. https://doi.org/10.1021/es60025a002.

Koch, Christian, Gauri M. Jog, and Ioannis Brilakis. 2013. "Automated Pothole Distress Assessment Using Asphalt Pavement Video Data." *Journal of Computing in Civil Engineering* 27 (4): 370–78. https://doi.org/10.1061/(ASCE)CP.1943-5487.0000232.

Lee, Jong Jae, Jong Won Lee, Jin Hak Yi, Chung Bang Yun, and Hie Young Jung. 2005. "Neural Networks-Based Damage Detection for Bridges Considering Errors in Baseline Finite Element Models." *Journal of Sound and Vibration* 280 (3–5): 555–78. https://doi.org/10.1016/j.jsv.2004.01.003.

Loulizi, Amara, I. L. Al-Qadi, and Mostafa Elseifi. 2006. "Difference between In Situ Flexible Pavement Measured and Calculated Stresses and Strains." *Journal of Transportation Engineering* 132 (7): 574–79. https://doi.org/10.1061/(ASCE)0733-

947X(2006)132:7(574).

Murase, Kimiya, and Kunihito Kato. 2018. “By Using Multidimensional Response Variables.”

Negulescu, Ioan, Louay Mohammad, William Daly, Christopher Abadie, R Cueto, Codrin Daranga, I Glover, et al. 2006. “Chemical and Rheological Characterization of Wet and Dry Aging of SBS Copolymer Modified Asphalt Cements: Laboratory and Field Evaluation.” *Asphalt Paving Technology: Association of Asphalt Paving Technologists-Proceedings of the Technical Sessions* 75: 267–96.

Rana, Sohel, Subramani P, Raul Fangueiro, and Antonio Gomes Correia. 2016. “A Review on Smart Self-Sensing Composite Materials for Civil Engineering Applications.” *AIMS Materials Science* 3 (2): 357–79. https://doi.org/10.3934/matersci.2016.2.357.

Schnebele, E., G. Cervone, and N. Waters. 2014. “Road Assessment after Flood Events Using Non-Authoritative Data.” *Natural Hazards and Earth System Sciences* 14 (4): 1007–15. https://doi.org/10.5194/nhess-14-1007-2014.

Wang, He, and William G Buttlar. 2018. “Three-Dimensional Analytical Model for Exploration of the Block Cracking Phenomenon in Asphalt Pavements.” *Road Materials and Pavement Design* 0 (0): 1–21. https://doi.org/10.1080/14680629.2018.1532923.

Xu, Wei, and Zhen Yang. 2018. “Infrared Spectroscopy Analysis of the Blending of Virgin and RAP Binders in Hot Recycled Asphalt Mixture with CTBN as Tracer.” *Journal of Testing and Evaluation* 47 (1). https://doi.org/10.1520/JTE20170302.

Yao, Hui, Zhanping You, Liang Li, Shu Wei Goh, Chee Huei Lee, Yoke Khin Yap, and

Xianming Shi. 2013. “Rheological Properties and Chemical Analysis of Nanoclay and Carbon Microfiber Modified Asphalt with Fourier Transform Infrared Spectroscopy.” *Construction and Building Materials* 38: 327–37. https://doi.org/10.1016/j.conbuildmat.2012.08.004.

Yu, X., and E. Salari. 2011. “Pavement Pothole Detection and Severity Measurement Using Laser Imaging.” *IEEE International Conference on Electro Information Technology*. https://doi.org/10.1109/EIT.2011.5978573.

Zhu, Chongzheng, Henglong Zhang, Guoqing Xu, and Chaofan Wu. 2018. “Investigation of the Aging Behaviors of Multi-Dimensional Nanomaterials Modified Different Bitumens by Fourier Transform Infrared Spectroscopy.” *Construction and Building Materials* 167: 536–42. https://doi.org/10.1016/j.conbuildmat.2018.02.056.